



## Probabilistic and physically-based modelling of rainfall-induced landslide susceptibility using integrated GIS-FORM algorithm

**Abstract** The susceptibility mapping of rainfall-induced landslides is an effective tool for predicting and locating disaster-prone zones at the regional scale. One of the most important parts of landslide susceptibility models is the hydrological model. In this context, the present study considers three pore water pressure (PWP) profiles with surface runoff to estimate the spatiotemporal variation of wetting front depth (WFD) during rainfall episodes. To reasonably simulate the inherent uncertainty and variability involved in the hydrogeomechanical properties of the surficial soil layers at the regional scale, probabilistic analysis based on the recursive first-order reliability method (FORM) is employed to calculate the probability of slope failure. The regional time-dependent landslide susceptibility mapping is realised using a newly developed model called Physically-based probabilistic modelling of Rainfall Landslides using Simplified Transient Infiltration Model (PRL-STIM). The proposed model is applied in a representative area that suffered extensive rainfall-induced landslides in July 2013 (Niangnianba Town, Gansu Province, China). The results indicate that the PRL-STIM model achieved a satisfactory prediction accuracy of 75% AUC compared to existing models like transient rainfall infiltration and grid-based regional slope-stability model (72%) and the probabilistic analysis results based on the first-order second moment method (74%). It also performed well in predicting the spatial distribution of shallow landslides, with a success rate of 81.6%. Regarding the model efficiency, the completion of a raster file for calculating the landslide probabilities of the study area (including 711,051 cells) requires only 17.1 s. It is thus hoped that the proposed calculation framework of PRL-STIM that considers various uncertainties (e.g., nonlinearity of the physical model, non-normal probability distributions, random variable cross correlations, etc.) in geotechnical parameters is better suited for landslide susceptibility mapping at the regional scale, where only limited historical event data is available.

**Keywords** Landslide susceptibility · Slope stability · Rainfall transient infiltration · Probabilistic analysis · First-order reliability method (FORM)

### Introduction

In the background of global warming and climate change, extreme rainfall events are no longer a scarcity (Kendon et al. 2023). Therefore, it is of paramount importance to investigate rainfall-induced landslides, which frequently pose significant natural hazards in mountainous regions (Emberson et al. 2021) and have the potential to cause immeasurable devastation (Haque et al. 2016). The initial step in addressing this issue involves conducting a landslide susceptibility

assessment, which aims to estimate the spatial probability of slope failures while considering potential governing factors that exhibit significant uncertainties and even spatial-temporal variations (Ji et al. 2022). Due to the complexity of uncertainty propagation and the necessity of accurate prediction of future events, probabilistic and/or statistical analysis methods often serve as the fundamental tool for producing landslide susceptibility results in those geohazard-vulnerable regions (Marin and Mattos 2020; Oguz et al. 2022). The quantitative methods for landslide susceptibility mapping can be generally summarised into two types (Gatto et al. 2023): (1) the ‘black box’ method embedding either the knowledge-driven or the data-driven methods using machine learning and statistical data mining techniques (Pham et al. 2016; Chae et al. 2017; Liu et al. 2023) and (2) the physically-based modelling (PBM) method that considers intrinsic failure mechanisms and available information of physical parameters (Li et al. 2022; Durmaz et al. 2023).

On the one hand, data-driven methods concentrate on analysing the associations between landslide prediction and triggering factors (Chang et al. 2023). Recently, the adoption of machine learning (ML)-based data-driven methods has been increasing. These approaches facilitate the development of rather accurate mathematical models that link causative factors to susceptibility levels utilising historical landslide databases (Pradhan 2013; Dou et al. 2020). It should be noted that, in regions with limited data availability, ML methods may encounter challenges in generating reliable results (Segoni et al. 2018; Huang et al. 2023). However, recent advancements in data-driven methods are addressing some of these challenges. For instance, Bordoni et al. (2021) have developed a novel data-driven approach based on the multivariate adaptive regression splines technique to dynamically forecast both spatial and temporal probabilities of rainfall-induced regional shallow landslides.

On the other hand, the PBM methods primarily focus on utilising the inherent mechanism of slope failure and its variation in response to changing environmental conditions, thus exhibiting enhanced capability and reduced application limitations. Consequently, they are frequently employed for quantitative evaluation of landslides at a regional scale (Fell et al. 2008). For predicting rainfall-induced shallow landslides, the analysis commonly focuses on modelling the change of groundwater table due to lateral flow or vertical flow of rainfall infiltration. Iverson (2000) combines the infinite slope stability calculation with a transient, one-dimensional analytical solution for pore pressure response to steady-state and transient rainfall infiltration. The infiltration model employed in transient rainfall infiltration and grid-based regional slope-stability model (TRIGRS) is based on the linearized solution introduced by Iverson and extended to Richards equation by Baum et al. (2002, 2008). In

addition, other well-known models such as the stability index mapping (SINMAP), shallow slope stability model (SHALSTAB), shallow landslides instability prediction (SLIP) and Scoops3D are also frequently employed in predicting rainfall-induced shallow landslides at the regional scale (Montgomery and Dietrich 1994; Pack et al. 1998; Montrasio et al. 2011; Tran et al. 2018). It is important to note that while models like SINMAP and SHALSTAB consider shallow translational landslides controlled by steady-state groundwater flow, the TRIGRS model focuses on slope failures occurring below the wetting front temporarily saturated due to rainfall infiltration (Zizoli et al. 2013). However, the assumption of steady-state flow may not be valid in regions characterised by highly variable rainfall patterns. The SLIP model assumes that slope instability is primarily attributed to the presence of partially saturated soils, which can be found either at the failure surface (soil-bedrock contact) or at a higher elevation. The Scoops3D evaluates the slope stability calculation by utilising the limit equilibrium method, such as the ordinary Fellenius or the simplified Bishop approach, based on the spherical failure surface (Reid et al. 2000, 2015). However, it does not incorporate the hydrological model.

To account for the distinct dynamics of surface and subsurface flows, rigorous rainfall infiltration models have been developed by integrating the hydrological and geotechnical characteristics of slopes with infiltration and seepage in recent years. The Green-Ampt model (1911) is one of the widely recognised PBMs for this purpose, and numerous studies have adapted it to include real-time precipitation data and changes in groundwater table over time, such as the YS model (Kim et al. 2014) and spatial prediction of rainfall-induced shallow landslides (SPRIn-SL) (Raimondi et al. 2023). Note that these models suit particularly for shallow landslides assuming a well-defined surficial soil depth above the bedrock. In general, hydrological models that describe shallow landslides can be categorised into two primary types that can be called 'vertical flow' and 'lateral flow' in a simple way. Medina et al. (2021) proposed an integrated approach considering both types to simulate the final water table position by accounting for the soil thickness, which is given by the depth of the soil-bedrock contact. However, in some cases of shallow landslides, the failure surface is not located at the soil-bedrock contact (Jiang et al. 2023). Additionally, more sophisticated rainfall-induced landslide models encompass the entire rainfall process by coupling the precipitation, infiltration, evaporation and transpiration processes (e.g. Rahardjo et al. 2007). For PBM of the regional landslide susceptibility, it is vital to emphasize the fast calculations while considering the complex processes of rainfall infiltration and surface runoff. As a computational trade-off, the one-dimensional Richards equation being further simplified by Lumb (1962) offers some novel insights for rapid rainfall mechanism calculations (Sun et al. 1998; Lee et al. 2009; Zhang et al. 2016). This aspect also constitutes a pivotal component of the PBM proposed in this paper.

Accurate susceptibility mapping of rainfall-induced shallow landslides at the regional scale is significantly challenging due to various uncertainties in geotechnical, geological and hydrological parameters (Zhang et al. 2014; Lee and Park 2015; Park et al. 2019). The probabilistic analysis integrated with PBM can comprehensively deal with those uncertainties for landslide susceptibility mapping (Zhang et al. 2018; Hwang et al. 2023). Several PBM methods, such as GEOTop-FS, HIRESSS and TRIGRS-P, have been

previously extended into probabilistic analysis by simulating a single parameter uncertainty (Simoni et al. 2008; Raia et al. 2014). Other widely employed probabilistic analysis techniques, such as the first order second moment (FOSM) and point estimation method (PEM), have also been utilised in probabilistic landslide susceptibility assessment (Kaynia et al. 2008; Park et al. 2017). However, these approaches exclusively assume the input parameters to follow the normal distribution to estimate the probability of failure (POF), which potentially overlooks the more realistic statistical distributions and correlations among random variables, and can lead to significant prediction errors. Monte Carlo simulation (MCS) was proposed as another possible tool for probabilistic analysis. The advantage of MCS is the fact that it approximates the probability of a specific event by simulating failure scenarios and random variables without the use of a probability density function. The application of MCS in landslide susceptibility assessment has been extensively explored (Broeckx et al. 2019; Li et al. 2022), including the utilisation of the TRIGRS model (Lee and Park 2015; Marin and Mattos 2020). However, given its nature as a computationally extensive simulation method, the MCS technique has exhibits inherent deficiencies when used for fast regional landslide susceptibility assessment with PBM. Considering the comprehensive nature of probabilistic information, including statistical distribution, correlation matrices of random variables and computational efficiency, leveraging the first-order reliability method (FORM) could be a viable approach. This method not only ensures rapid convergence but also accommodates potential non-normal distributions and parameter cross-correlation. However, only a limited number of studies have addressed the simultaneous achievement of fast and accurate prediction of shallow landslides by employing physical models and efficient probabilistic algorithms.

The previous literature review reveals two primary hurdles with existing landslide susceptibility models: hydrological modelling and physical parameter uncertainties. Many existing hydrological models often fail to balance quick computational speed with the accurate simulation of complex processes, particularly rainfall infiltration and surface runoff, which are essential for region-scale shallow landslide predictions. Moreover, despite the proficiency of MCS and similar probabilistic methods in addressing parameter uncertainty, their computational demands pose practical limitations on their application for regional probabilistic landslide susceptibility analysis.

The main goal of this study is to present a novel PBM approach that can effectively capture the failure mechanisms of rainfall-induced shallow landslides by integrating a simplified hydrologic model of transient infiltration and a probabilistic approach for the soil properties. The approach is named 'Physically-based probabilistic modelling of Rainfall Landslide using Simplified Transient Infiltration Model (PRL-STIM)'. We notably investigate the temporal variations in wetting front depth (WFD) resulting from transient infiltration induced by rainfall, while accounting for surface runoff. To enhance the computational efficiency, the rainfall infiltration is estimated using an approximate solution derived from the one-dimensional Richards model. Finally, the fast batch probabilistic analysis based on the recursive algorithm of the FORM is employed to effectively produce the probability of PBM landslides over regional areas, thereby providing a practical framework for conducting rainfall-induced landslide susceptibility mappings.

Furthermore, the practical feasibility of the proposed model will be demonstrated through its application to the Niangniangba area landslides in China.

## Study area and data source

### General settings

The study area in Niangniangba Town is located in the southern foothills of the western Qinling Mountains, Gansu Province, China. It is characterised by rugged terrain with complex valleys and mountains. The small basin in the northeastern section of Niangniangba Town is the focal study area as depicted in Fig. 1 following a relative literature report (He et al. 2021). This basin covers an area of 53.81 km<sup>2</sup>, and the elevation ranges from 1416 to and 2138 m a.s.l., with an average elevation of 1777 m a.s.l. (Fig. 2a).

The surface layer comprises Quaternary strata with a complex origin, including both landslide accumulation layer ( $Q_4^{del}$ ) and

diluvial layer ( $Q_4^{pal}$ ) deposits. The  $Q_4^{pal}$  strata are limited to the residual valley terrace and have a loose structure and low density. The soil layer is relatively thin and underlain by various rock strata including Pleistocene Malan loess, Neogene mudstone and sandstone, Anshan period granite, Upper Devonian slate, and quartz sandstone (He et al. 2021). This geological composition increases the susceptibility of this study area to new landslides during rainfall.

The study area, situated in a transition zone between semi-humid and semi-arid climates, features a temperate continental climate with an average annual relative humidity of 66% and an average annual precipitation of 500.7 mm (1981–2010). Eighty-five percent of the annual precipitation falls between April and October; specifically, the period from July to September experiences the most concentrated precipitation, contributing 68% of the annual total. Consequently, heavy rainfall is identified as the primary factor in triggering geological disasters in this study area.

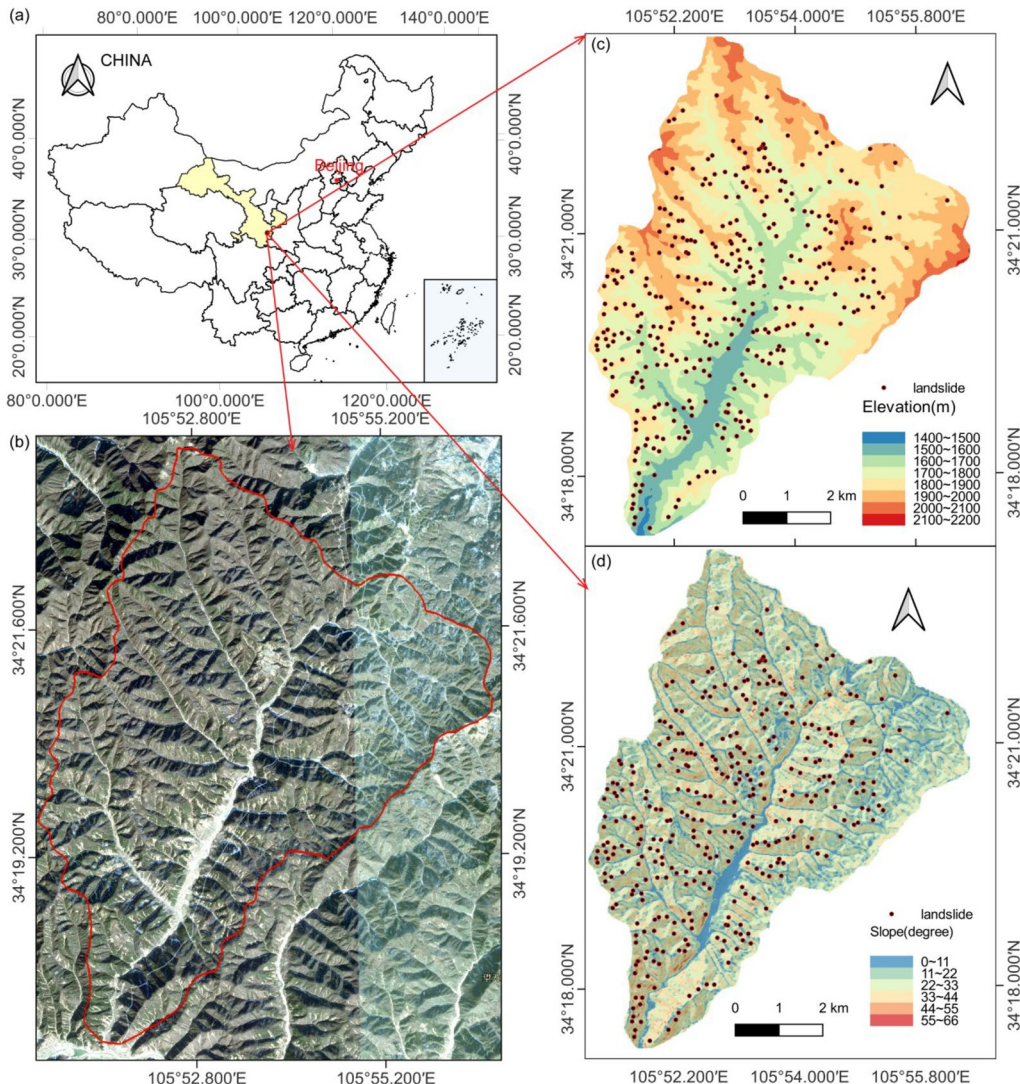


**Fig. 1** The Niangniangba study area. **a** Location inside China. **b** Google Earth image. **c** Digital elevation model (DEM). **d** Slope angle map including the landslides observed during the 2013 episode

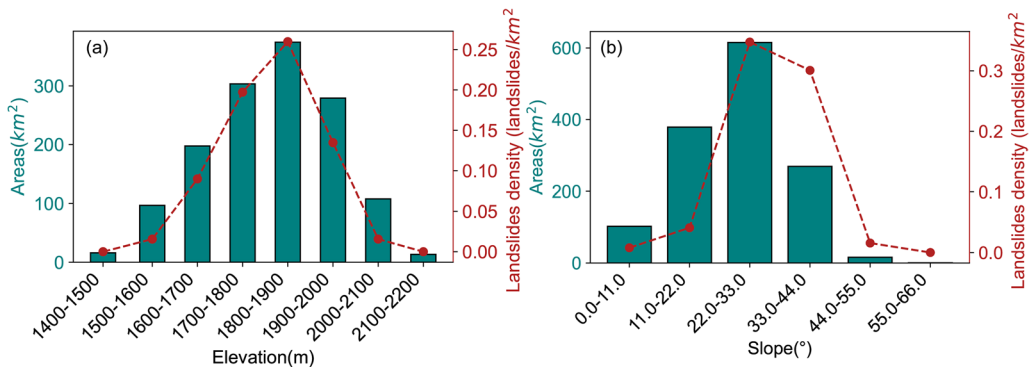


**Fig. 2** Effect of elevation (a) and slope angle (b) on landslide occurrence in the Niangniangba study area during the 2013 episode

### The 2013 landslide episode

The catastrophic geological hazards resulting from this rainfall primarily consist of shallow landslides characterised by a mix of weathered rock and gravelly soil on a small scale (He et al. 2021). The clustering pattern of landslides shown in Figure 1c is evident following the occurrence of rainfall events. Notably, the orientation of the underlying mudstones aligns with the slope direction. Composed of weathered rocks and gravelly soil, these landslides typically have a thickness not exceeding 3 m and exhibit significant regional and clustering characteristics. An inventory of shallow landslides was obtained following the results of He et al. (2021), while recent Google Earth images were used to identify the detailed locations of actual landslides in remote areas of Niangniangba Town. Most landslides are observed between 1506 and 2047 m a.s.l. (Fig. 2a). The terrain slope varies from 22° to 33°, which makes it more prone to landslides (Fig. 2b).

In the month preceding the landslide, the study area underwent four heavy rainfall events, which triple the average for that period. The cumulative rainfall from 21 to 23 July amounted to 104.3 mm. To accurately assess the slope instability and the potential for landslides due to heavy rainfalls, we simulated the rainfall commencing exactly at noon on the day. This timing is optimal to encompass the actual rainfall period, which, as indicated in Fig. 3, extends from 12:00 pm on July 21 to 6:00 am on July 22.

### Data availability

The PRL-STIM model proposed in this study requires three main types of input parameters: topographic parameters (elevation, slope angle, flow direction) derived from the digital elevation model (DEM), geotechnical parameters and rainfall information. The model utilises a 12.5-m-resolution DEM downloaded from ALOS PALSAR (<https://search.asf.alaska.edu>). The original DEM was

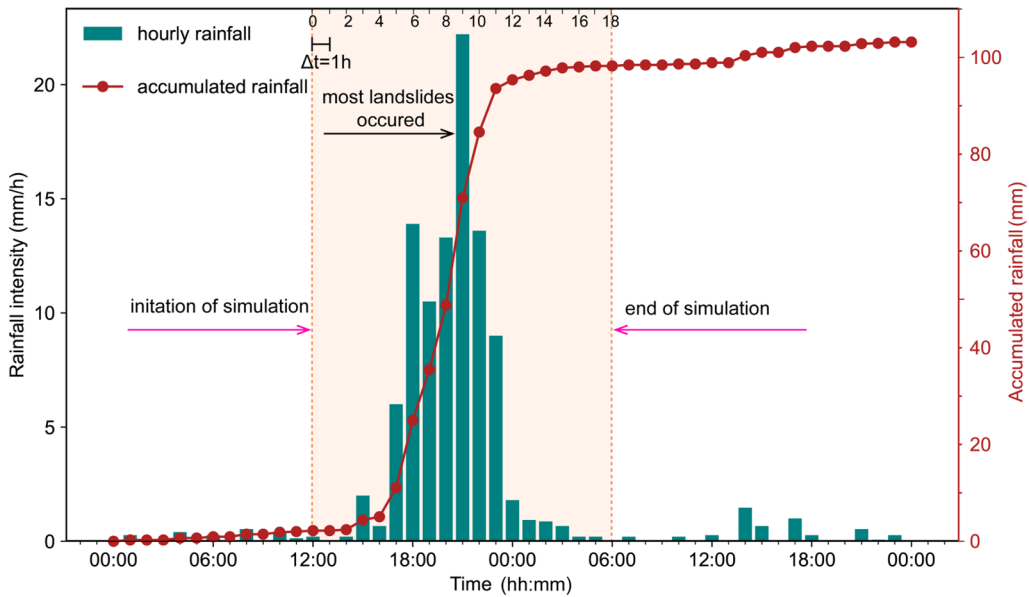


**Fig. 3** Rainfall conditions during the July 2013 episode

filled to produce the raster file of topography and earth slopes. This process is automatically performed by the PRL-STIM v1.0 software. The single-flow D8 algorithm determines the flow direction of the cell grid, thus completing the entire processing of the required data.

Additionally, the spatial data of soil thickness and soil type are necessary for PRL-STIM as well. The covered soil varies from areas of direct bedrock exposure to locations with a sedimentary depth of several meters. According to He et al. (2021), the region is predominantly characterised by drab soil and brunisolic soil, primarily composed of loamy-silty clay, accounting for over 80% of the land area. The soil thickness in the study area typically ranges from 0.1 to 3.0 m. The geological and soil conditions in all regions are similar. Therefore, the corresponding soil type is treated as a single class as listed in Table 1. The model parameters adopted including soil porosity ( $n$ ), saturated unit weight of soil ( $\gamma_{\text{sat}}$ ), saturated coefficient of permeability ( $k_s$ ) and rainfall intensity ( $I_R$ ) are listed in Fig. 3. It should be noted that the initial and final degrees of saturation ( $S_0$  and  $S_f$ , respectively) can be calculated based on the initial and final volumetric water content, as referenced in He et al. (2021). The detailed transformation formula is presented in section ‘The hydrological model’.

## Methodology

### Model description

#### The infinite slope theory

The infinite slope model calculates the factor of safety (FS) based on limit equilibrium analysis and is suitable for assessing shallow landslides with planar failure surfaces. It has been widely used to evaluate susceptibility for rainfall-induced landslides with shallow failure surfaces parallel to the slope and integrated with GIS for regional-scale analysis. In this study, some reasonable assumptions are made as follows: (1) the sliding surface is parallel to the slope surface, (2) the sliding surface overlaps with the rainfall infiltration wetting front ( $z_w$ ) and (3) infiltration seepage in the soil is considered. (4) The WFD should not exceed the maximum soil depth.

First of all, to describe the variation of WFD ( $z_w$ ) caused by the rainfall infiltration, the Mohr–Coulomb criteria incorporating unsaturated soil strength with three different PWP profiles were adopted, as outlined by Rahardjo et al. (1995). As shown in Fig. 4, profile A represents the situation where the matric suction is reduced to zero at the ground surface and the suction increases with depth until it reaches the hydrostatic line at depth  $z_w$ . This also illustrates a gradual advancement of the wetting front, which is commonly encountered in fine-grained soils. Profile B portrays a distinct advancement of the wetting front, which is frequently encountered in soils of coarse-grained soils. Profile C exhibits a temporary rise of the groundwater table, which is often observed in soils with a high-permeability layer above and a lower-permeability layer below the wetting front.

In general, the three different PWP profiles can be formulated as follows (Huang et al. 2022):

$$u_w(z) = \begin{cases} -\frac{z}{z_w}\gamma_w h_c & \text{for profile A} \\ 0 & \text{for profile B} \\ \gamma_w z(\cos\beta)^2 & \text{for profile C} \end{cases} \quad (1)$$

where  $u_w$  is the PWP at a vertical depth of  $z$  ( $0 \leq z \leq z_w$ ),  $\gamma_w$  is the unit weight of water,  $h_c$  is the initial suction head at  $z=z_w$  before rainfall infiltration,  $h_c = (H - z_w)\cos^2\beta$  and  $\beta$  denotes the slope angle.

The effective shear strength of the soil ( $\tau_f$ ) is given by

$$\tau_f = c' + \sigma \tan\phi \quad (2)$$

where  $c'$  and  $\phi'$  denote the soil effective cohesion and friction angle, respectively.

The total normal stress and shear stress at the base of the sliding soil element are

$$G = (\gamma_{\text{sat}} \times z_w + q_t) \cos^2\beta \tau = (\gamma_{\text{sat}} \times z_w + q_t) \sin\beta \cos\beta \quad (3)$$

where  $\gamma_{\text{sat}}$  denotes the saturated unit weight of soil, the uniform load of the tree is set as  $q_t$  and  $z_w$  denotes the WFD.

**Table 1** Selected values of soil parameters

Soil class	Parameters	Unit	Probability distribution	COV	Mean ( $\mu$ )	Standard deviation
Drab soil and brunisolic soil	$c_s$	kN/m <sup>2</sup>	Normal	0.10, 0.20, 0.30	18.5	$\sigma = \mu \text{ COV}$
	$\phi$	°			20	
	$n$	–			0.12	
	$S_f$	–			1	
	$S_0$	–			0.67	
	$\gamma_{\text{sat}}$	kg/m <sup>3</sup>			25	
	$\log(k_s)$	m/h			0.000025	
	$h_s$	m			$h_{si}^a$	

COV coefficient of variation

<sup>a</sup>The mean of  $h_s$  is assumed to be the value obtained from the soil depth model calculation

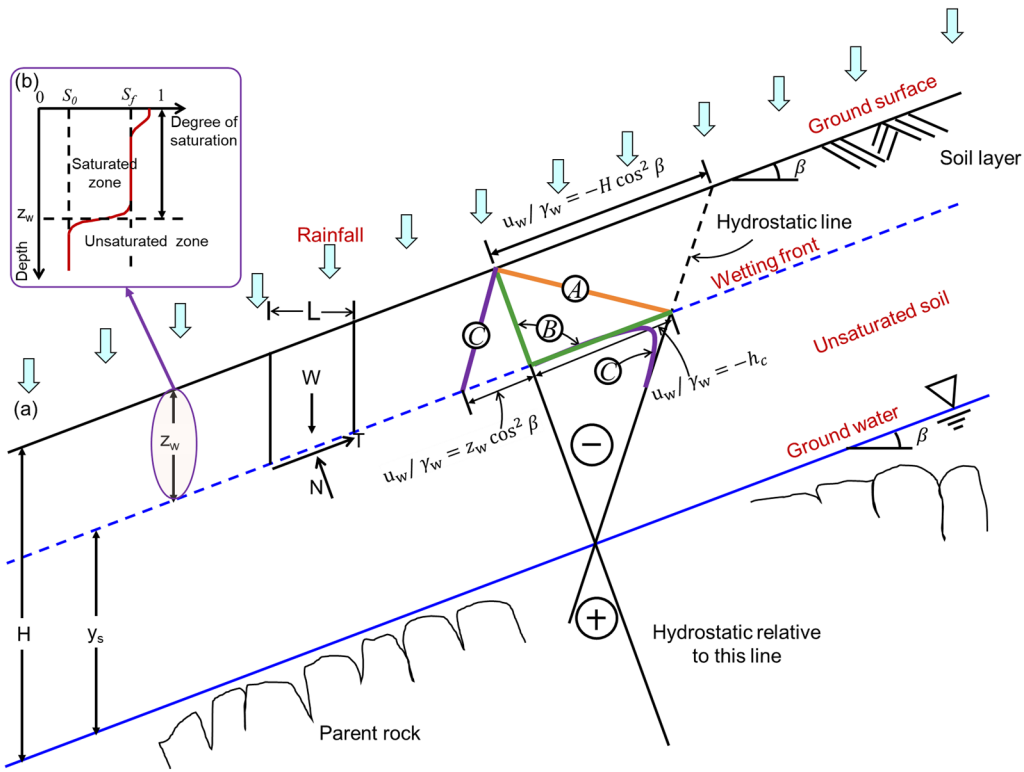


**Fig. 4** The rainfall-infiltration infinite slope stability model incorporating unsaturated soils and three PWP profiles. **a** Overview of PWP profiles A, B and C (adapted from Rahardjo et al. (1995)). **b** Variation of the degree of saturation with soil depth (adapted from Lumb (1962))

The resistive shear stress developed at the sliding base can be given by

$$\tau_d = c'_d + \sigma' \tan \phi'_d = c_d' + (\sigma - \chi u_w) \tan \phi_d' \quad (4)$$

where  $c'_d$  and  $\phi'_d$  denote the mobilised strength parameters (the cohesion and the angle of friction, respectively, that develop along the potential failure surface), and  $\chi$  is the effective stress parameter (Huang et al. 2022).

Thus, combining Eq. (3) with Eq. (4)

$$\tau_d = c'_d + (\gamma_{sat} z_w \cos^2 \beta + q_t \cos^2 \beta - \chi u_w) \tan \phi_d' \quad (5)$$

At the limit equilibrium state, Eq. (5) can be written as

$$(\gamma_{sat} z_w + q_t) \sin \beta \cos \beta = c'_d + (\gamma_{sat} z_w \cos^2 \beta + q_t \cos^2 \beta - \chi u_w) \tan \phi_d' \quad (6)$$

The FS can be calculated by considering the relationship between mobilised strength and effective strength (Cui et al. 2022)

$$\left\{ \begin{array}{l} \tan \phi'_d = \frac{\tan \phi'}{FS} \\ c'_d = \frac{c'}{FS} \end{array} \right. \quad (7)$$

Or

$$FS = \frac{c'}{\gamma_{sat} \times z_w \sin \beta \cos \beta} + \frac{\tan \phi'}{\tan \beta} - \frac{\chi u_w}{\gamma_{sat} \times z_w \sin \beta \cos \beta} \frac{\tan \phi'}{\tan \beta} \quad (8)$$

where  $c' = c'_s + c'_r$ , and  $c'_s$  and  $c'_r$  denote the soil cohesion and root cohesion, respectively.

For simplicity, the  $c'_r$ ,  $q_t$  is neglected in this study, and the FS can be described as follows:

$$FS = \frac{c'_s}{(\gamma_{sat} \times z_w + q_t) \sin \beta \cos \beta} + \frac{\tan \phi'}{\tan \beta} - \frac{\chi u_w}{\gamma_{sat} \times z_w \sin \beta \cos \beta} \frac{\tan \phi'}{\tan \beta} \quad (9)$$

Therefore, Eq. (9) is the general expression of FS for the PWP profiles shown in Fig. 4a, and  $u_w$  is calculated by Eq. (1) with  $z = z_w$ . The effective stress parameter  $\chi = 1$  is adopted for saturated soil slopes (Huang et al. 2022).

It is worth pointing out that the upper bound FS value for a given infiltration length ( $z_w$ ) can be determined based on profile B

$$FS = \frac{c'_s}{\gamma_{sat} \times z \sin \beta \cos \beta} + \frac{\tan \phi'}{\tan \beta} \quad (10)$$

In contrast, the identical thickness of the groundwater table would yield different results for the same infiltration length when using PWP profile B (e.g. in FSLAM (Medina et al. 2021))

$$FS = \frac{c'_s}{\gamma_{sat} \times z \sin \beta \cos \beta} + \left( 1 - \frac{z_w}{z} \frac{\gamma_w}{\gamma_{sat}} \right) \frac{\tan \phi'}{\tan \beta} \quad (11)$$

Note that another well-known physically-based model is the TRIGRS model, which assesses pore water pressure responses

perpendicular to the slope surface under varying rainfall intensities and timings, accounting for both transient and steady states during heavy rainfall (Iverson 2000). This model generates diagrams that illustrate the pressure head distribution for each period by integrating temporal and spatial dimensions (Ji and Cui 2023). The model utilises digital terrain to evaluate the slope stability at the regional scale based on the infinite slope (Montgomery and Dietrich 1994). In this model, for an approximately infinite slope, the sliding surface of each grid extends indefinitely. It treats every fixed depth as a plane parallel to the ground while disregarding forces between adjacent grid cells in the sliding mass. The FS of each grid cell can be calculated as follows (Baum et al. 2002, 2008):

$$FS(z, t) = \frac{\tan \phi'}{\tan \beta} + \frac{c' - \Psi(z, t)\gamma_w \tan \phi'}{\gamma_{sat} z \sin \beta \cos \beta} \quad (12)$$

where  $\Psi(z, t)$  denotes the ground-water pressure head as a function of depth  $z$  and time  $t$ .

#### The hydrological model

Although the governing one-dimensional transient flow in unsaturated soil can be expressed by the conceptual infiltration model, this model is widely employed to assess slope instability based on the WFD and PWP profiles. The soil under rainfall is fully saturated near the surface, and near-saturated ( $S_f = 0.8$  to  $0.9$ ) down to a depth of  $z_w$ . For long duration and heavy rainfall, the diffusion of infiltrated water can be neglected and the analytical solution of  $z_w$  which resulted from the one-dimensional Richards equation is given as follows (Lumb 1962; Zhang et al. 2011; Huang et al. 2018):

$$z_w = \frac{k_s t}{n(S_f - S_0)} \quad (13)$$

where  $k_s$  is the saturated coefficient of permeability,  $n$  is the soil porosity,  $S_f$  is the final degree of saturation and  $S_0$  is the initial degree of saturation.

Equation (13) is appropriate when encountering the case of  $I_R \geq k_s$  where  $I_R$  denotes the rainfall rate (m/h). Based on this, a generalized wetting front equation was proposed by Sun et al. (1998). The corresponding  $z_w$  can be expressed as follows:

$$z_w = \frac{I_R t}{\theta_s - \theta_0} \quad (14)$$

where  $\theta_0$  is the initial volumetric water content corresponding to the  $u_0$ , and  $\theta_s$  is the final volumetric water content.

The parameters  $n$  and  $S_0$  are not explicitly given and are referred to the soil water characteristic curve (SWCC) in Zhang et al. (2011, 2016)

$$\begin{cases} S_f = \frac{\theta_s}{n} \\ S_0 = \frac{\theta_0}{n} \end{cases} \quad (15)$$

In the case of rainfall intensity,  $I_R$  will change with time and the  $z_w$  is evaluated through a modified infiltration model according to Eqs. (13), (14) and (15)

$$z_{wti} = z_{wti(i-1)} + \Delta z_{wti} \quad (16)$$

where  $z_{wti}$  denotes the WFD at  $t_i$ , and  $\Delta z_{wti}$  denotes the increased WFD at  $t_i$ . Meantime, the  $\Delta z_{wti}$  can be rewritten by introducing a component of  $\cos \beta$  (Lee et al. 2009)

$$\begin{cases} \frac{k_s \Delta t}{(\theta_s - \theta_0) \cos \beta}, I_R \geq k_s \\ \frac{I_R \Delta t}{(\theta_s - \theta_0) \cos \beta}, I_R \geq k_s \end{cases} \quad (17)$$

Note that the  $z_{wti}$  is controlled by the entire depth of the soil ( $h_s$ )

$$z_{wti} = \begin{cases} h_s, z_{wti} \geq h_s \\ z_{wti}, z_{wti} \geq h_s \end{cases} \quad (18)$$

#### Runoff model

Following the TRIGRS model (2002, 2008), the infiltration ( $I_R$ ) is calculated at each cell as the sum of the precipitation ( $P$ ) and any upslope cell runoff ( $R_u$ ), subject to the constraint that it must not exceed the saturated hydraulic conductivity ( $k_s$ )

$$I_R = \begin{cases} P + R_u, P + R_u < k_s \\ k_s, P + R_u \geq k_s \end{cases} \quad (19)$$

At each cell where  $P + R_u$  exceeds  $k_s$ , the excess is considered runoff ( $R_d$ ) and is diverted to an adjacent downslope cell.

$$R_d = \begin{cases} P + R_u - k_s, P + R_u - k_s > 0 \\ 0, P + R_u - k_s < 0 \end{cases} \quad (20)$$

The final infiltration ( $I$ ), which is different from the rainfall intensity ( $I_R$ ), can be calculated by considering the saturated hydraulic conductivity as follows:

$$I = \begin{cases} k_s, I_R \geq k_s \\ I_R, I_R < k_s \end{cases} \quad (21)$$

#### Determination of the soil thickness of shallow landslides

Determination of the potential soil thickness is a challenging task for shallow landslide analysis on the regional scale (Segoni et al. 2012). The soil depth is frequently assumed to be a constant value across the full area when applying the infinite slope in the assessment of regional slope stability. There are some empirical models of the soil cover thickness to determine the spatial distribution of the soil thickness in the research region and therefore estimate the possible sliding depth of potential shallow landslides (Saulnier et al. 1997), for example the GIST model (Catani et al. 2010; Segoni et al. 2012) and topographic-based models, such as Z-model, S-model and Sexp model (Salciarini et al. 2006; Tran et al. 2018). Additionally, recent advancement has seen the integration of machine learning algorithms with the empirical model (GIST-RF) which is a significant step forward in estimating soil thickness, as demonstrated by Xiao et al. (2023).

The Z-model is widely recognised as a simplistic approach and has been also extensively utilised in numerous studies to ascertain soil thickness (Li et al. 2022; Hwang et al. 2023). To achieve fast regional landslide susceptibility assessment, we have chosen to adopt the Z-model in this study as well

$$Z_{model} : h_i = h_{max} - \frac{Z_i - Z_{min}}{Z_{max} - Z_{min}}(h_{max} - h_{min}) \quad (22)$$

where  $h_{max}$  and  $h_{min}$  are the maximum and minimum soil thickness, respectively;  $Z_i$  is the elevation of a cell; and  $Z_{max}$  and  $Z_{min}$  are the maximum and minimum elevation, respectively.

#### Implementation of FORM with HLRF-x recursive algorithm

The computation of FS using Eq. (9) can be very fast, thus making it possible for regional landslide prediction. However, the model input parameters are by no means deterministically available at a regional scale. To account for these uncertain input parameters, the physical model in terms of FS can be mathematically extended into the probabilistic description, such that:

$$P_f = \int_{g(\mathbf{x}) < 0} f(\mathbf{x}) d\mathbf{x}, \text{ with limit state function (LSF)} : g(\mathbf{x}) = FS(\mathbf{x}) - 1 \quad (23)$$

where  $P_f$  is the POF, the vector  $\mathbf{x} = (c_s, \tan\theta, \beta, n, \gamma_{sat}, \dots)$  denoting a collection of random variables (of input parameters),  $f(\mathbf{x})$  is the joint probability distribution function of random variables  $\mathbf{x}$  and  $FS(\mathbf{x})$  is a functional format of Eq. (9).

This integral equation for  $P_f$  is nearly impossible to solve at speed, not to mention for regional landslide analysis. Alternatively, an efficient approximate solution known as the FORM can be adopted, which has the following necessary recipes:

$$P_f = \Phi(-\beta_f) \quad (24)$$

$$\beta_f = \sqrt{\left[ \frac{x_i^* - u_i^N}{\sigma_i^N} \right]^T \mathbf{R}^{-1} \left[ \frac{x_i^* - u_i^N}{\sigma_i^N} \right]} \quad (25)$$

where  $\Phi(\cdot)$  denotes the standard normal cumulative distribution function,  $\beta_f$  is called the reliability index,  $x_i^*$  denotes the most probable failure point (MPP) value of  $i^{th}$  random variable (denoted in terms of random variable  $\mathbf{x}$ ) and  $u_i^N$  and  $\sigma_i^N$  denote the equivalent normal mean and standard deviation of the  $i^{th}$  variable, respectively, and they contain important information of  $\mathbf{x}$ 's semi-probability distribution functions;  $\mathbf{R}$  is the correlation matrix. A detailed explanation can be found in Low and Tang (2007).

FORM is a semi-probability calculation method that is well known in geotechnical engineering failure analysis. The fundamental concept of the FORM probabilistic calculation is to find the reliability index (RI) evaluated at the MPP's  $\mathbf{x}$  values. In this work, we adopt the fast recursive algorithm HLRF-x proposed by Ji and Kodikara (2015) to implement the FORM calculation into GIS. In brief, the HLRF-x recursive algorithm for locating the MPP in the space of random variables defined by vector  $\mathbf{x}$  ( $x$ -space) is written as follows:

$$\mathbf{x}_{k+1} = \boldsymbol{\mu}_k^N + \frac{1}{\nabla g(\mathbf{x}_k)^T T_k \nabla(\mathbf{x}_k)} [\nabla g(\mathbf{x}_k)^T (\mathbf{x}_k - \boldsymbol{\mu}_k^N) - g(\mathbf{x}_k)] T_k \nabla g(\mathbf{x}_k) \quad (26)$$

where  $\mathbf{T}_k = [\sigma_k^N]^T \mathbf{R} [\sigma_k^N]$  is the transformation matrix,  $\mathbf{x}_k$  is the vector of random variables in  $x$ -space and  $\boldsymbol{\mu}_k^N$  is the vector of equivalent MV to convert random variables into the normal distribution.

Furthermore, the diagonal matrix  $\sigma_k^N = \begin{bmatrix} \sigma_{k,i}^N & \cdots & 0 \\ \vdots & \ddots & \vdots \\ 0 & \cdots & \sigma_{k,m}^N \end{bmatrix}$ ,  $\sigma_{k,i}^N$  is the equivalent normal standard deviation of the  $i^{th}$  random variables evaluated at  $\mathbf{x}_k$  and  $\mathbf{R}$  is the correlation matrix of all random variables.  $\nabla g(\mathbf{x}_k)$  denotes the gradient vectors of the LSF evaluated at  $\mathbf{x}_k$ .

On the other hand, the FOSM is another popular probabilistic approach for processing the uncertainty resulting from the input parameters in regional landslide susceptibility assessment (Marin et al. 2021). This method is based on the Taylor series expansion of the performance function about the mean value, using directly the mean value and partial derivative of the LSF to evaluate the failure probability. Other complicated statistical information of the random variables, such as the distribution type, and the correlation between random variables are ignored and, hence, may lead to unrealistic prediction results.

#### Brief description of PRL-STIM v1.0

##### General overview

The fast batch computation of POF using the FORM with the HLRF-x algorithm in the GIS platform may encounter some challenges that are not discussed in other uncertainty propagation methods such as FOSM or MCS. For example, the recursive algorithm used by HLRF-x requires multiple calculations, which are difficult to perform using standard grid computations in popular GIS-related software such as ArcGIS; analysing the necessary dataset for topographic and geomorphological parameters is time-consuming and often requires utilising geospatial technology on multiple software platforms. To overcome these challenges, we developed a Windows-based software that allows users to automatically perform the probabilistic PBM and generate landslide susceptibility mappings, named 'the PRL-STIM v1.0'. The software workflow is shown in Fig. 5.

##### Software inputs and outputs

Herein, the input data and output results required for this software are briefly mentioned. The software allows users to import frequently used file formats: raster and text files, i.e., .tif and .csv. These input files include the DEM, the maximum and minimum value of soil depth, mechanical and hydraulic property data, physical parameter data with statistical information, and spatial distribution of soil types. A correlation matrix ( $\mathbf{R}$ ) can be imported as a separate CSV file. The CSV files used for landslide susceptibility distribution parameters must include seven columns with the corresponding probability distribution parameter values. Parameters defining ten common types of probability distributions are referred to relevant literature (Low and Tang 2007).

The software outputs include FS, WFD, soil depth, RI and POF, as well as CDF of POF files. The software will automatically process raster datasets that include soil cohesion, friction, slip depth, slope angle and unit weight, among others. The rainfall model was automated in this software to obtain the WFD and to evaluate FS using Eqs. (9), (15),

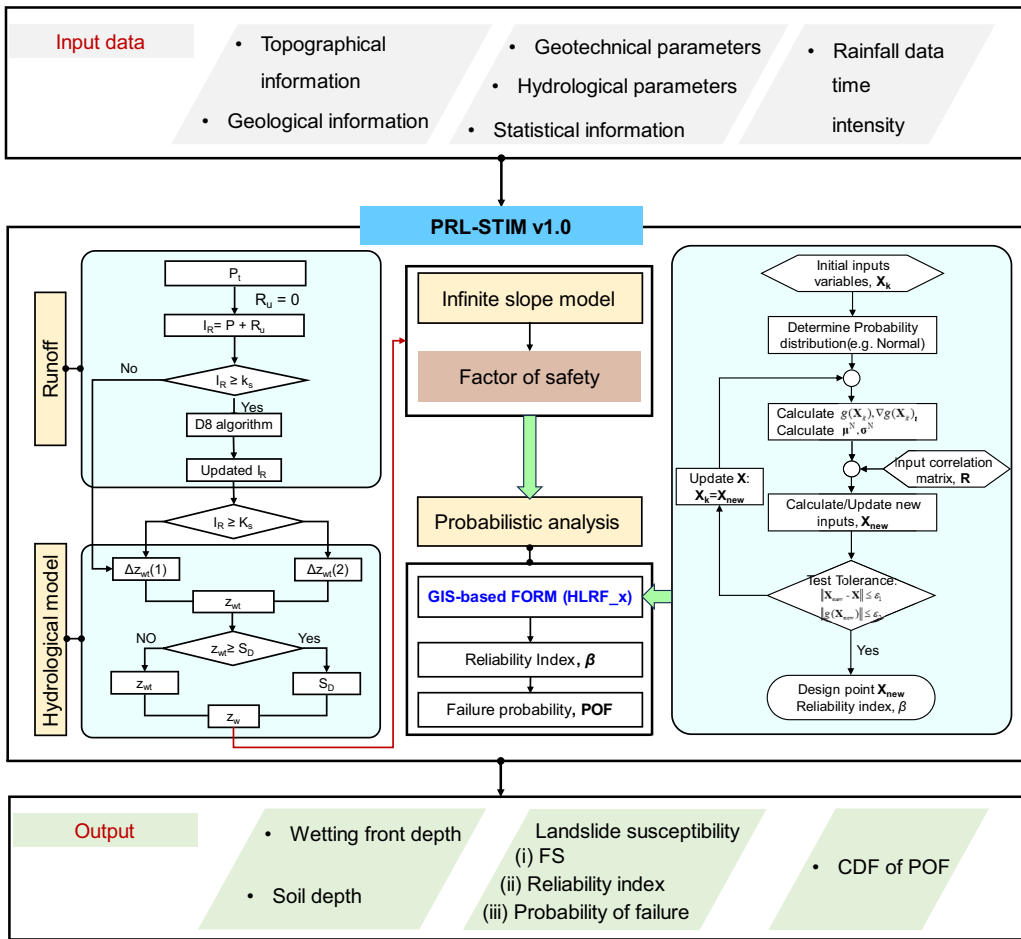


**Fig. 5** Flow chart illustrating the work process of PRL-STIM v1.0

(16), (17) and (18). Probabilistic analysis was conducted using the GIS-FORM with HLRF-x recursive algorithm, as illustrated in Fig. 5. The POF of each array element was estimated, and the results were written automatically to raster files. These outputs generate a series of raster layers for a rapid geological hazard assessment.

#### Sensitivity analysis of PRL-STIM

To evaluate the potential impact of each input variable on the resulting FS value and to identify the most effective variables for probabilistic simulation, such as FORM, the sensitivity analysis is conducted for the PRL-STIM model. The ranges of physical parameter values used for the sensitivity analysis are listed under the ‘Values’ and ‘Default value’ columns, as detailed in Table 2.

It is noted that beneath the Niangniangba area, a low-permeability layer underlies the loamy-silty clay, which may hinder deep water infiltration and lead to a perched water table above the bedrock. The upper soil layer is susceptible to saturation during rainfall, and slow drainage may be observed due to the reduced permeability of the underlying stratum. Water accumulation between these layers may increase pore water pressure in the upper soil, potentially causing landslides. Thus, profile C is chosen as the

representative PWP profile for this study (Fig. 4) and corresponding results are presented as well.

#### Assessment of model performance

To assess the model’s performance, we employ both the widely recognised ROC analysis and the  $\%LR_{class}$  index. Additionally, the results of the TRIGRS model are used for comparative analysis. Furthermore, to enhance the accuracy assessment of probabilistic models, we incorporate the FOSM method along with the FORM within the probabilistic analysis module of PRL-STIM.

#### ROC analysis

The ROC analysis and its corresponding area under the ROC curve (AUC) are widely employed as the most significant metrics for assessing model performance. This index offers a balanced analysis of model accuracy and false positive rate (FPR), with higher AUC values indicating better prediction performance. Balanced accuracy (BA) and accuracy (ACC) are also utilised as the evaluation index. The probability of detection (POD) is also calculated by comparing the number of true positive detections with the total number of actual targets, such as observed landslides. The resulting value ranges from 0 to 1, with a higher value indicating

**Table 2** Parameters values for model verification and susceptibility

Parameter type	Parameter	Unit	Values	Default value
Rainfall intensity	$I_R$	mm/h	0.2/3/4/52	52
Geometry	$\beta$	°	15/22.5/30/37.5/45	30
	$h_s$	m	0.1/1.0/1.5/2.0/2.5/3.0	3.0
Soil	$c_s$	kN/m <sup>2</sup>	9.25/13.875/18.5/23.125/27.75	18.5
	$\phi$	°	16/24/32/40/48	32
	$n$	—	0.06/0.09/0.12/0.15/0.18	0.12
	$S_f$	—	0.6/0.7/0.8/0.9/1.0	1
	$S_0$	—	0.27/0.37/0.47/0.57/0.67	0.67
	$\gamma_{sat}$	kg/m <sup>3</sup>	12.5/18.75/25/31.25/37.5	25
	$\log(k_s)$	m/s	0.005/0.00036/0.000025/0.00000167/0.0000125	0.000025

better performance of the model. In contrast to the ROC curve, the POD focuses solely on the number of correctly detected targets. In this study, to avoid predicting stable regions as unstable, namely neglecting the existence of false positives, we have additionally chosen 5000 random points within the non-landslide region (i.e. actual stabilisation areas) to improve the model test.

#### Landslide ratio index (%LR<sub>class</sub>)

Apart from the aforementioned indexes, the LR<sub>class</sub> index has also been widely utilised to assess the performance of PBM (Salciarini et al. 2017). The LR<sub>class</sub> (landslide ratio for each predicted FS class) proposed by Park et al. (2013) illustrates the correlation between the percentage of landslides within a specific class (FS or POF compared to the landslide inventory) and the corresponding percentage of area predicted as landslides in each FS or POF class, considering that areas of failure may not necessarily be present within these classes.

$$LR_{class} = \frac{\% \text{ of contained landslide locations in each FS/POF class}}{\% \text{ of predicted landslide areas in each FS/POF class}} \quad (27)$$

The %LR<sub>class</sub> was introduced by Tran et al. (2018) through modification of Eq. (27). It preserves the initial definition of the numerator as the percentage of slope failure locations included in each FS grade, which should be computed based on the number of landslides per FS/P<sub>f</sub> grade rather than the number of failure grid cells (Park et al. 2013). The FS grades for this study were determined based on stable and unstable conditions. Two FS grades were utilised: FS < 1 (representing unstable conditions) and FS ≥ 1 (indicating stable conditions). Regarding POF, various classes were examined. The LR<sub>class</sub> percentage index for the FS<sub>i</sub> class represents the corresponding proportion of the total LR<sub>class</sub> value among all FS<sub>i</sub> classes. A larger value of %LR<sub>class</sub> means better model performance, i.e. higher prediction accuracy.

$$\%LR_{class}^i = \frac{LR_{class}^i}{\sum_{i=1}^n LR_{class}^i} \quad (28)$$

#### Analysis of results

##### Results from the sensitivity analyses of model parameters

The sensitivity analysis revealed several interesting outcomes regarding the model's behaviour. As shown in Fig. 6, the FS values exhibit significant variations across the rainfall intensity ( $I_R$ ) range of 1.23 to 59.22 which highlights the crucial role of rainfall conditions. Consequently, the sensitivity analysis outcomes unequivocally establish that the parameter of rainfall intensity holds utmost significance within this proposed model. In addition, the corresponding FS also exhibits obvious variations immediately afterwards, ranging from 1.23 to 26.50, solely by adjusting the value of  $k_s$ . The subsequent significant change in sensitivity was observed in soil depth ( $h_s$ ). Specifically, as  $h_s$  increased from 0.01 to 3, the corresponding FS decreased from 17.75 to 1.23. This indicates that the model performance will be influenced by soil depth. For the remaining parameter, the FS change is also more significant when adjusting the terrain slope. However, as the slope is derived from the DEM, it is not included in the sensitivity analysis. For soils with a permeable layer (i.e. profile C), subsequent findings have demonstrated the pivotal influence of friction angle on slope stability. Furthermore, soil cohesion also exerts a substantial impact on slope stability. Conversely, the impact of saturation weight on the model appears to be relatively insignificant. The initial saturation and porosity exhibit negligible effects on the model when compared to other parameters.

In summary, while most physical parameters play significant roles in this rainfall-induced shallow landslide model, it is crucial to properly define  $k_s$ ,  $h_s$ ,  $c$ ,  $\phi$  and  $S_f$ , based on the results of Fig. 6.

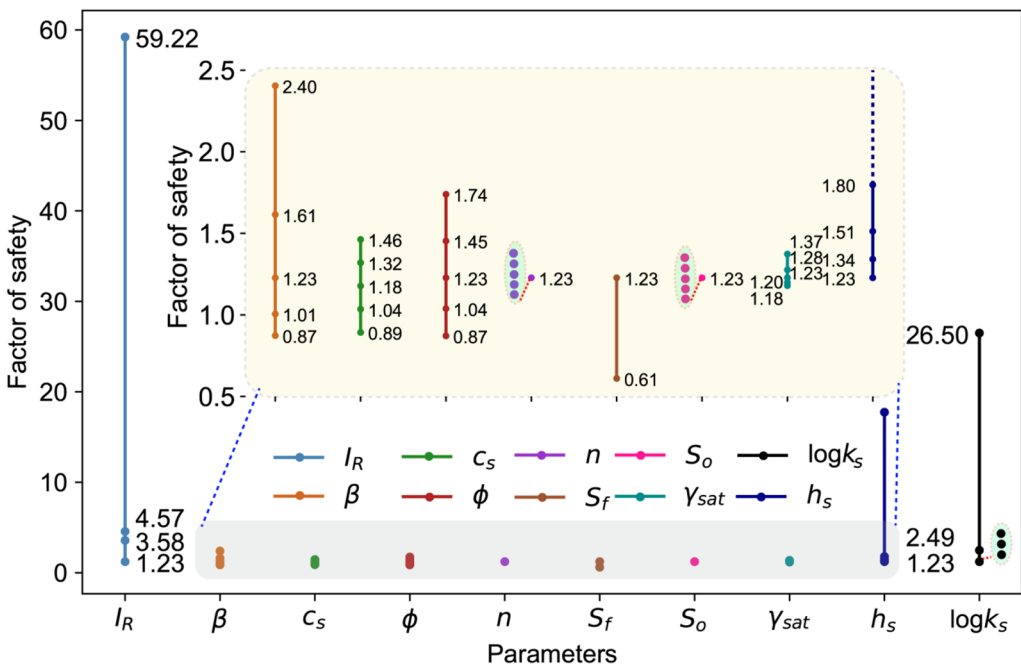


**Fig. 6** Sensitivity of the input parameters of the proposed model considering the PWP profile C (the calculated FS value is added next to each dot). Each dot indicates a parameter value listed in Table 1

## Results of the application to the study area

The main results revealed several interesting outcomes regarding the application of proposed PRL-STIM which include the wetting front depth and the deterministic and probabilistic landslide susceptibility assessment.

### Analysis of WFD

The WFD was computed through the proposed model based on the hourly rainfall intensity, as well as the geotechnical and hydrogeological parameters. Figure 7a–h illustrates the spatial distribution of the WFD at different time instants. The minimum WFD is 0.1 m below the ground as shown in Fig. 7a, and values of 0.01 ~ 0.07 m dominate the research area, which represents the relatively dry condition after rainfall 3 h. These results suggest that after 3 h of rainfall infiltration, the WFD is still shallow. Figure 7d shows the spatial distribution of WFD after 6 h of rainfall infiltration, with most WFD values between 0.1 and ~ 0.15 m. Nevertheless, the sharp increase in rainfall intensity, as depicted in Fig. 7a, led to a rapid augmentation in WFD (as shown in Fig. 7i), thereby exacerbating instability across the entire study area. Figure 7f shows the spatial distribution of WFD after 9 h of rainfall, and the maximum value reaches 2.7 m, which means that the rainfall water infiltrates nearly the entire soil thickness. Furthermore, Fig. 7i shows the changes and trend of the ratio between WFD and soil depth (SD) at different rainfall durations from 0 to 16 h. After 9 h of rainfall infiltration, the WFD/SD reached the maximum value and remained stable thereafter, which implies the soil was saturated. It is worth noting that this specific time (21:00) corresponds to the period during which the

highest number of recorded landslides was reported (He et al. 2021). The relationship between WFD and slope stability will be further discussed in section ‘Deterministic versus probabilistic analysis’.

### Deterministic versus probabilistic analysis

For simplicity, we ignored the statistical correlations between uncertain model parameters in this section and used a coefficient of variation (COV) value of 0.3 to compare deterministic and probabilistic simulation results. The specific model parameters are presented in Table 1.

To effectively illustrate the deterministic outcomes of varying landslide susceptibility levels during the rainfall episode, as shown in Fig. 8, we present the proportionate variation of unstable areas with continuous rainfall. Figure 8 shows the tempo-spatial distributions of landslide susceptibility at the beginning, after 6 h and 9 h of rainfall infiltrations. Overall, it shows that the landslide susceptibility in terms of FS increases significantly with the rainfall duration. The WFD increases slowly during the first 4 h of rainfall, and the unstable area is almost zero. After 6 h of continuous rainfall (17:00), only a negligible proportion of the area (0.4%) exhibited an FS < 1.0. Subsequently, at the end of 6 h of rainfall, there was a noticeable increase in potentially unstable regions, accounting for approximately 12% of the total area surveyed. The incidence of failure areas continued to escalate rapidly and reached a significant level (38%) after 9 h of precipitation exposure. The fact that the proportion of unstable areas remains unchanged despite continuous rainfall is noteworthy.

Figure 9 shows the probabilistic analysis results. Specifically, the selection of a suitable POF threshold is significant for evaluating the landslide susceptibility. The five following threshold levels were adopted: I (very low)  $POF \leq 0.01$ , II (low)  $0.01 < POF \leq 0.1$ , III

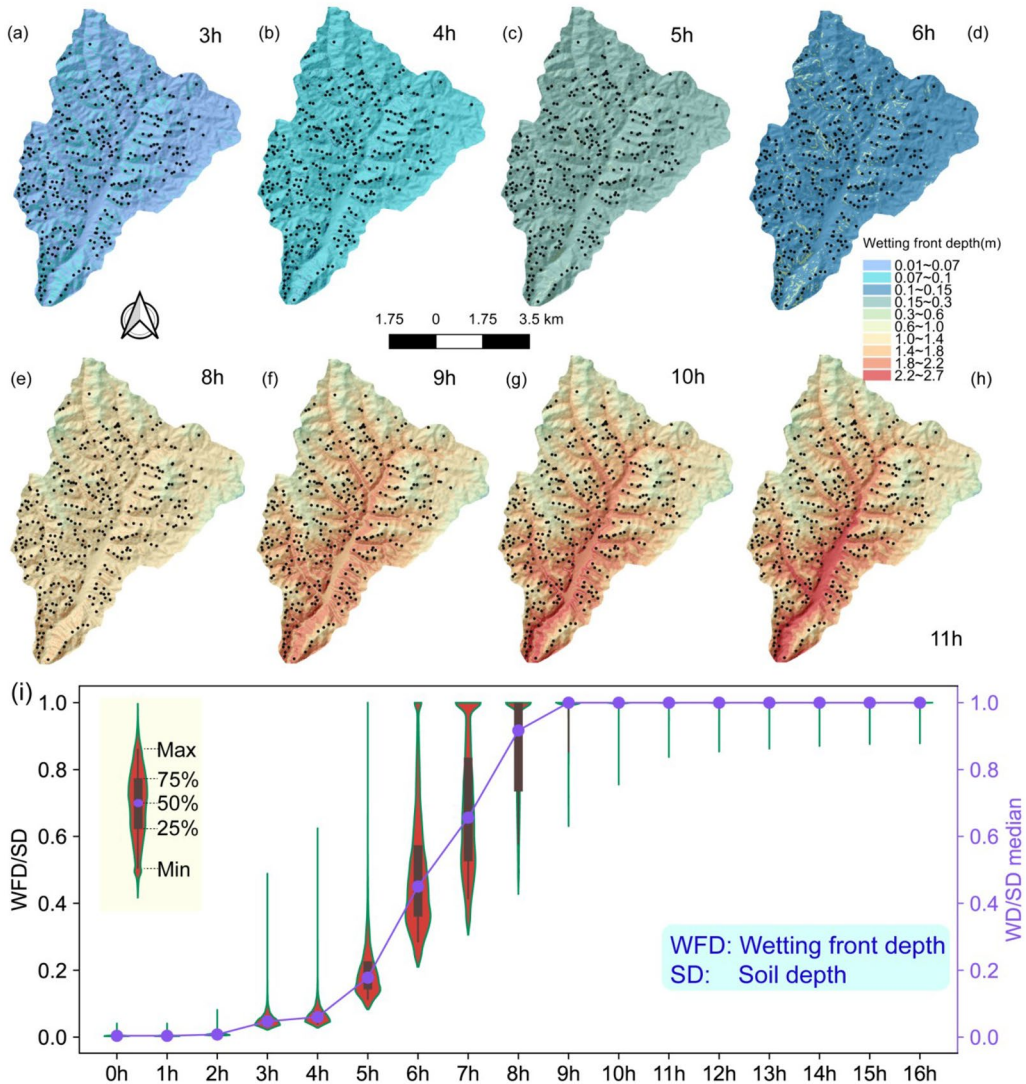


**Fig. 7** Temporal evolution of WFD during the rainfall episode. **a–h** Maps of WFD from 4 to 12 h after rainfall initiation. **i** Ratio between wetting front and soil depth in the entire study area

(moderate)  $0.1 < \text{POF} \leq 0.5$ , IV (high)  $0.5 < \text{POF} \leq 0.9$  and V (very high)  $\text{POF} \geq 0.9$  (Ji et al. 2022). To investigate the temporal variation in probabilistic landslide susceptibility, we present the proportionate variation of unstable areas with continuous rainfall under different POF thresholds. As shown in Fig. 9, the proportion of unstable areas is already close to 100% after 5 h of rainfall when POF was set as 0.1. This indicates the POF threshold value is obviously unreasonable. For the case of using a POF threshold of 0.9, the proportion of unstable areas is not significant; i.e. the unstable areas are less than 1% after 9 h of rainfall. This also clearly implies the value is unsuitable. Instead, a POF threshold of 0.5 predicts a very noticeable region of instability, which is considered a significant threshold for regional probabilistic landslide susceptibility assessment in this study. This value has also been adopted in other relevant literature (Silva et al. 2008; Medina et al. 2021).

After 4 h of continuous rainfall (i.e. at 16:00), it was observed that none of the study areas exhibited  $\text{POF} > 0.5$ , indicating overall stability across the entire region. However, by the 6-h mark, there was a notable surge in the proportion of potentially unstable regions, reaching approximately 10%. Subsequently, due to persistent heavy precipitation, roughly 33% of the study area was classified as high-susceptibility regions by the 9-h mark (i.e. 21:00). This trend continues to the end of the rainfall with approximately 34% of areas remaining unstable, as depicted in Fig. 9.

Regarding the predicted landslides (Figs. 8, 9) utilising the PRL-STIM, the evolution of potential landslides (unstable areas) of this case study can be broadly categorised into three distinct phases:

Stage I: From the onset of rainfall until 4 h, the intensity of precipitation remained low, resulting in a cumulative rainfall of only 9.1 mm. We contend that achieving soil saturation and the formation of a sliding surface at this stage poses a considerable challenge.

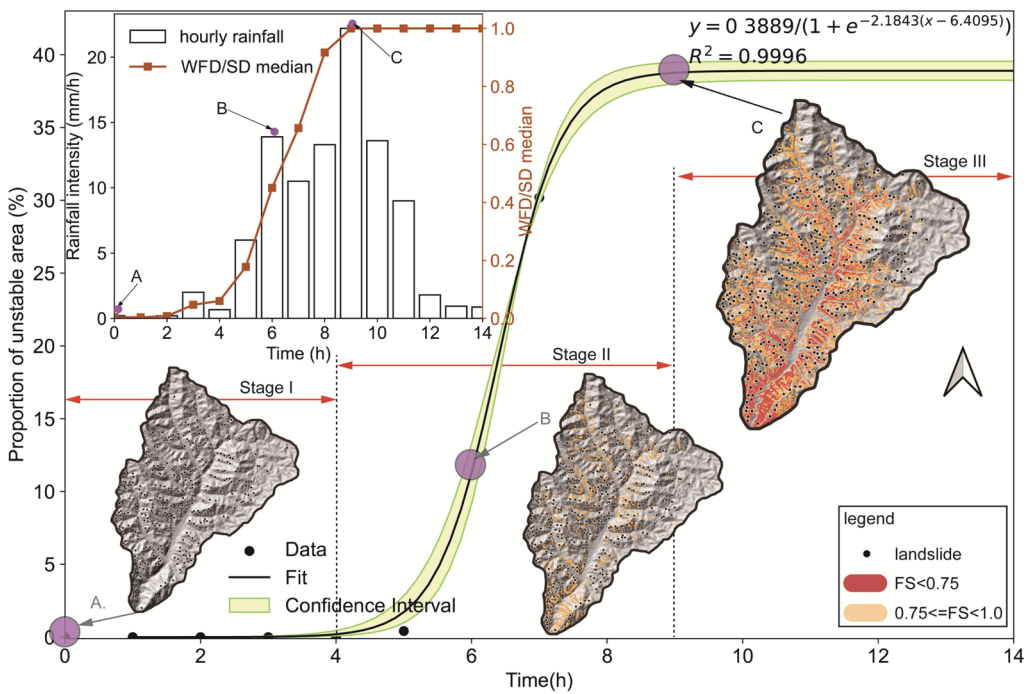


**Fig. 8** Results of the deterministic analysis. Time evolution of the unstable areas and three landslide susceptibility maps (at the beginning of the rainfall and 6 h and 9 h after the rainfall). Inset shows the change of WFD/SD ratio during the rainfall episode

Additionally, low-intensity rainfall provides insufficient external conditions for the occurrence of shallow landslides.

**Stage II:** The occurrence of landslides was predominantly observed during periods of heavy rainfall. Within a span of 5 h,

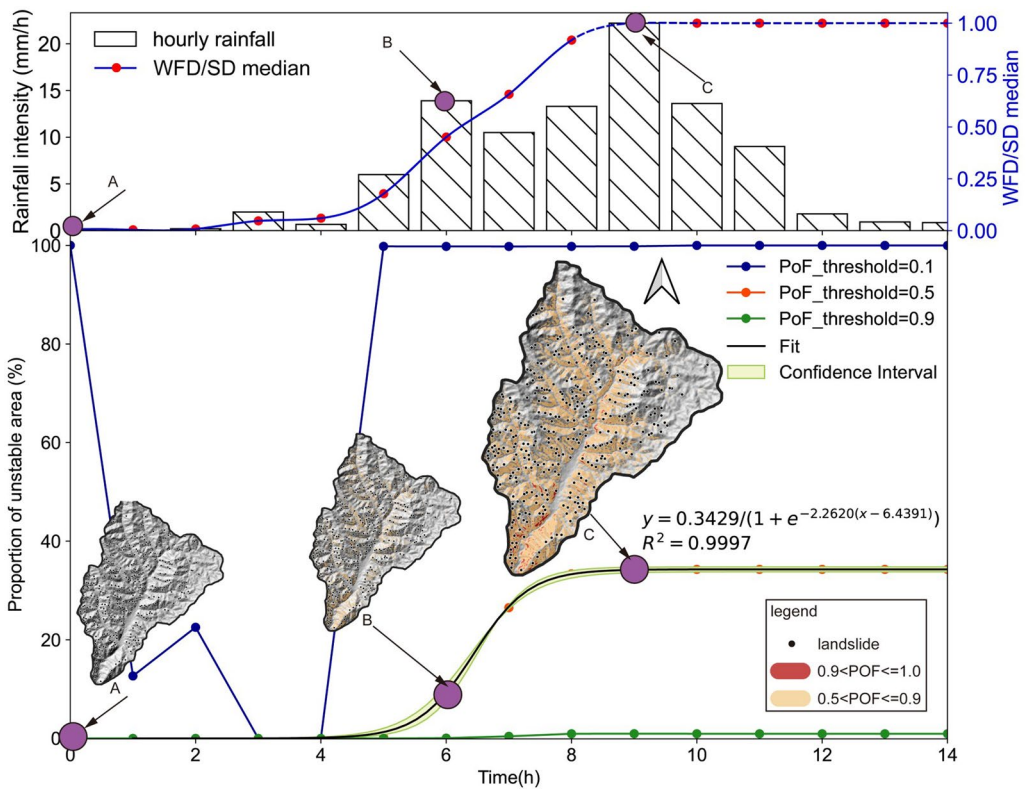


**Fig. 9** Results of probabilistic analysis. Time evolution of the unstable areas and three landslide susceptibility maps (at the beginning of the rainfall and 6 h and 9 h after the rainfall). The upper plot shows the change of WFD/SD ratio during the rainfall episode

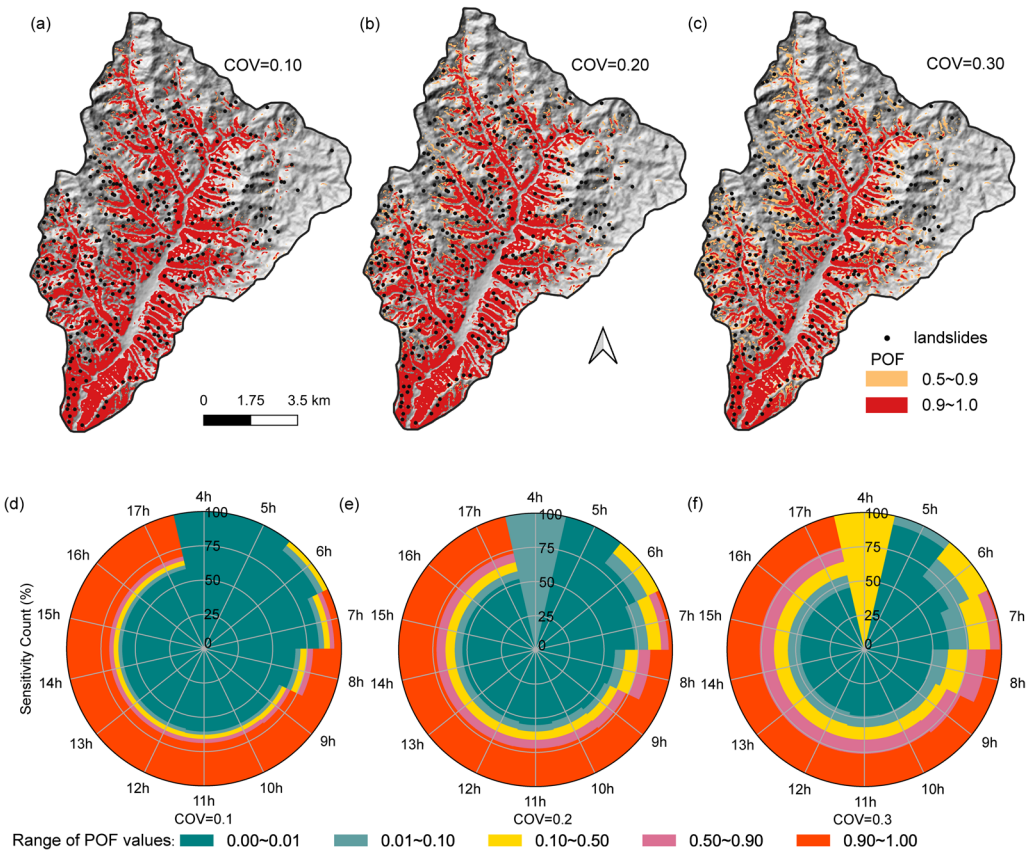


**Fig. 10** Probabilistic landslide susceptibility analysis under different COVs. POF spatial distribution map. **a** COV = 0.1. **b** COV = 0.2. **c** COV = 0.3. Percentage of the total study area with different susceptibility areas at different rainfall moments. **d** COV = 0.1. **e** COV = 0.2. **f** COV = 0.3

from the 4th to the 9th hour after rainfall initiation, there was an escalation in hourly precipitation intensity from 6 to 13.6 mm, accompanied by a cumulative increase in rainfall from 9.4 to 82.3 mm. The combination of intense precipitation within a short duration and pre-existing substantial rainfall led to rapid saturation of the shallow topsoil layer, resulting in a significant reduction in rock and soil mass stability and a subsequent dramatic rise in landslide probability.

Stage III: After the 10th hour, rainfall continues persistently, resulting in the WFD aligning with the soil body depth, indicating a fully saturated state of the soil body. Consequently, no new external factors contribute to sliding forces according to Eq. (9) and thus there is no further alteration in the unstable area.

The aforementioned discussion visually demonstrates changes in landslide susceptibility areas during rainfall using PRL-STIM, thereby providing a scientific foundation for real-time early-warning systems for rain-induced landslides.

#### Probabilistic results considering COVs in the proposed rainfall model

Probability analysis relies on the correct identification of uncertainty in the input data, and a key factor in the accuracy of predicted POF is the COV for the input data.

To assess the impact of different COVs (0.10, 0.20 and 0.30), we assumed all parameters followed a normal distribution and

compared their effects on landslide susceptibility at 23:00 local time (after 11 h, final condition). As mentioned earlier, a threshold POF value of 0.5 was deemed appropriate. Therefore, our initial focus lies on areas with POF values exceeding 0.5. Figure 10a–c illustrates that the spatial distribution of landslide sensitivity becomes more significant with an increase of COV.

As depicted in Fig. 10d–f, the variations in different susceptibility levels with rainfall over time were observed under three COVs. At the 5-h mark, the majority of areas were classified as having low susceptibility ( $\text{POF} \leq 0.01$ ). Notably, all areas exhibited a POF below 1% at a COV of 0.1. As the COV increased to 0.2, approximately 99.9% of areas were identified as having very low susceptibility ( $0.01 < \text{POF} \leq 0.1$ ). When the COV reached 0.3, nearly all areas (99.4%) were categorised as having moderate-level susceptibility due to parameter uncertainties that indicated potential slope failure in the future despite relatively high values of FS ( $> 1.5$ ). This further emphasizes the importance of considering parameter variability in probabilistic landslide susceptibility analysis.

The sensitivity of landslides exhibits distinct trends across different COV values. From a probabilistic analysis perspective, the standard deviation represents the dispersion or variability of data, while the COV indicates the relative magnitude of this dispersion by normalizing it with respect to the mean. A higher COV in a normal distribution suggests greater variability. Distributions with higher COVs may exhibit wider tails in their probability density

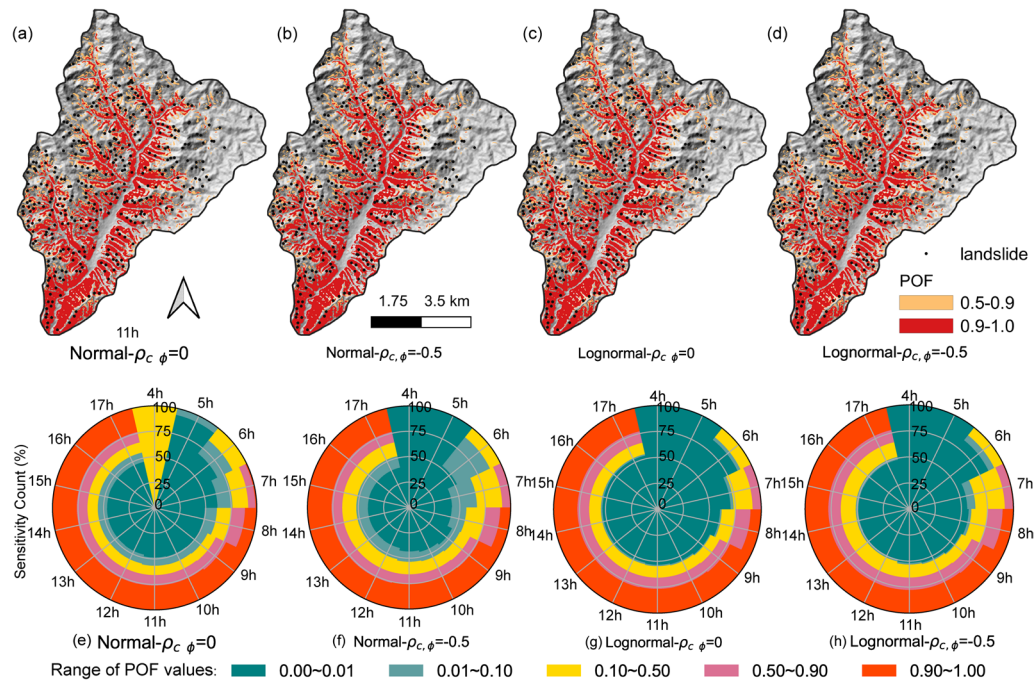


**Fig. 11** Probabilistic landslide susceptibility analysis under parameter correlations and non-normal distribution. POF distribution map. **a** Normal:  $\rho_{c,\phi} = 0$ . **b** Normal:  $\rho_{c,\phi} = -0.5$ . **c** lognormal:  $\rho_{c,\phi} = 0$ . **d** lognormal:  $\rho_{c,\phi} = -0.5$ . Percentage of the total study area with different susceptibility levels for increasing rainfall duration. **e** Normal:  $\rho_{c,\phi} = 0$ . **f** Normal:  $\rho_{c,\phi} = -0.5$ . **g** lognormal:  $\rho_{c,\phi} = 0$ . **h** lognormal:  $\rho_{c,\phi} = -0.5$

function, thereby increasing the likelihood of landslide occurrence due to exceptionally large values present in these tails. Therefore, when conducting regional probabilistic landslide analysis, careful consideration must be given to parameter COVs as they play a crucial role.

#### Probabilistic results accounting for statistical correlation and non-normal distribution

Accurate probabilistic landslide susceptibility assessment necessitates the consideration of interdependencies among potential physical parameters associated with landslides. In the case of landslides, multiple random variables such as terrain elevation, rainfall and

soil type may affect POF, especially for parameters like soil cohesion ( $c$ ) and friction angle ( $\phi$ ) that do not follow a normal distribution. Hence, to ensure accurate landslide susceptibility analysis, it is imperative to simultaneously consider correlation and non-normal distribution in determining POF.

To achieve this, it is ideal to adopt the lognormal distribution for simulating the distributions of  $c$  and  $\phi$ , as suggested by Ji and Kodikara (2015). Assuming that the remaining parameters are deterministic allows for investigating a negative correlation between  $c$  and  $\phi$  without any interference from other random variables. To incorporate the impact of correlation on probability landslide analysis, a negative correlation coefficient of  $-0.5$  was considered.

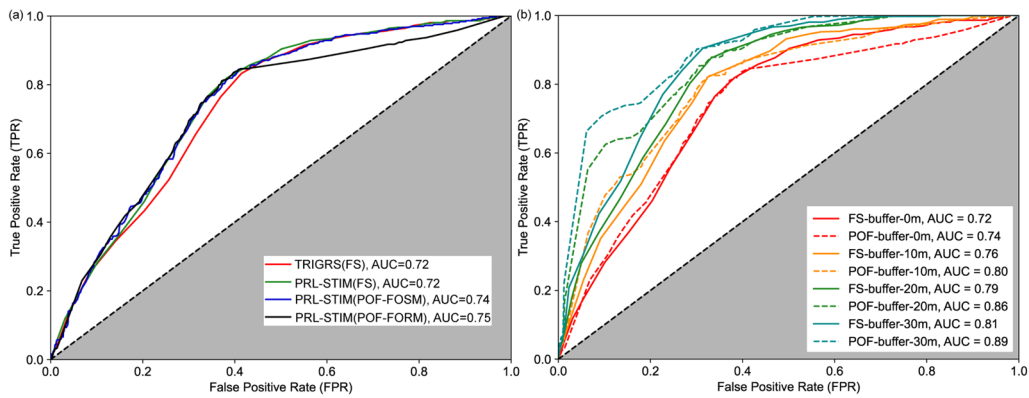


**Fig. 12** Results of the ROC analysis for the inventory of the 2013 landslide episode comparing the 'Factor of Safety' and 'Probability of Failure'. **a** ROC curves and AUC values of TRIGRS and PRL-STIM (FS and POF). **b** ROC curves and AUC values with/without buffer zone around inventory points

Figure 11a-d depicts the outcomes observed at 23:00, following 11 h of rainfall. It is noteworthy that employing different statistical distributions, such as normal and lognormal, featuring varied cross-correlations, can result in discrepancies in the POF in the context of regional probabilistic landslide assessments. Figure 11e-h illustrates the temporal changes in susceptibility levels associated with rainfall for three different parameter distributions, considering both correlated and uncorrelated parameters. At the 5-h mark, a majority of areas exhibited moderate susceptibility, with nearly 100% likelihood for the normal distribution (with a COV value of 0.3), compared to no areas showing very low susceptibility for the lognormal distribution. When considering correlated parameters, regardless of whether they followed a normal or lognormal distribution, almost all areas were classified as having low susceptibility levels.

Regarding the correlation of parameters, the stronger the negative correlation of the parameters, the more sensitive the distribution of the POF. This means that the potential of landslides increases as the correlation of parameters increases. Consequently, minor inaccuracies in determining the value of a single parameter will have a more substantial influence on the other parameter. This heightened sensitivity renders POF highly responsive to even slight modifications in parameter values.

## Discussion

The primary objective of this study was to investigate the feasibility of employing probabilistic physically-based modelling for regional-scale prediction of rainfall-induced shallow landslide susceptibility proposing a simple and fast solution. While there have been numerous successful applications of probabilistic PBM in predicting rainfall-triggered shallow landslides, few studies have achieved a balance between computational efficiency and prediction accuracy. In this study, we propose a novel PBM approach called PRL-STIM, which successfully captures the mechanism of rainfall-induced shallow landslides. This new model not only accounts for temporal variations in WFD resulting from transient infiltration induced by rainfall, but also incorporates the consideration of surface runoff. In addition, a fast batch probabilistic analysis based on the recursive algorithm of the FORM is employed to effectively estimate the probability of landslide occurrence over large areas.

## Comparison of performance analysis for different models

### Comparison based on ROC analysis

The underlying assumption of our proposed model is that the rainfall-induced shallow landslide occurrence is closely related

to the WFD. To assess the model's performance, we employed the predicted outcomes following an 11-h rainfall event, which corresponds to the time (23:00) when the number of landslides becomes constant. Additionally, we utilised the well-established TRIGRS as a benchmark for result analysis and conducted a comparative assessment of probabilistic outcomes using FOSM.

Specifically, we adopted the basic physical parameters for TRIGRS modelling, including slope, soil depth, unit weights of water and soil, cohesion, internal friction, saturated hydraulic conductivity, diffusivity and both saturated and residual soil water content, as described in section '[The infinite slope theory](#)'. The detailed values have been documented in Table 1, which were also utilised by He et al. (2021). By inputting the rainfall intensity at different time points, the TRIGRS model automatically computes the corresponding FS and pore pressure head ( $\psi$ ) at various moments. A noteworthy aspect is that the current TRIGRS model does not account for the uncertainty of input parameters, thus limiting its applicability solely to deterministic analyses.

Therefore, to compare the performance of FORM in PRL-STIM, the FOSM was introduced as a probabilistic alternative method, with its fundamental concept elucidated in section '[Implementation of FORM with HLRF-x recursive algorithm](#)'. The same probabilistic parameters and statistical distribution were adopted, including cohesion and internal friction with a COV value of 0.3. It should be noted that while the FOSM method is commonly used for landslide susceptibility mapping (Kaynia et al. 2008), it only considers uncorrelated normal distributions for input parameters. Therefore, default normal parameters were employed for cohesion and internal friction in this study using both FOSM and FORM methods in PRL-STIM. The specific values are listed in Table 1.

The ROC curve is the highly significant and widely used method for evaluating model performance in prediction modelling. The AUC value can be utilised to quantitatively compare the predictive capabilities of PBM models. Figure 12a displays the ROC curves of different models investigated in this study. The corresponding AUC values for FS-based TRIGRS, FS-based PRL-STIM, POF-based PRL-STIM (FOSM) and POF-based PRL-STIM (FORM) models are 0.72, 0.72, 0.74 and 0.75, respectively. It can be shown that both POF-based PRL-STIM (FOSM) and POF-based PRL-STIM (FORM) models generally exhibit superior predictive performances compared to their FS-based counterparts (TRIGRS and FS-based PRL-STIM), indicating increased sensitivity when considering parameter uncertainties probabilistically. FORM demonstrates higher prediction accuracy than FOSM under identical conditions. Additionally, regardless of employing different mechanisms to simulate rainfall

**Table 3** Confusion matrix comparing the effect of different buffers when using the POF=0.5 as the threshold of safety level of slope stability

Radius of buffer zone	TP	TN	FP	FN	FPR	POD	AUC	BA	ACC
0	284	1577	826	81	0.344	0.778	0.726	0.622	0.672
10 m	580	1552	742	137	0.323	0.809	0.757	0.743	0.708
20 m	2507	1580	739	442	0.319	0.850	0.791	0.766	0.776
30 m	5847	1535	722	741	0.320	0.888	0.814	0.784	0.835

infiltration, the deterministic predictive performance of PRL-STIM remains acceptable or even comparable to TRIGRS.

As shown in Fig. 12b, the AUC value can further be improved after applying a buffer zone around the landslide points (due to the uncertainty in the landslide inventory). When the buffer zone is 30 m, the AUC value increased to 0.81 and 0.89 based on FS and POF, respectively. Since the landslide inventory of the 2013 episode has relatively low precision, adopting a buffer zone is reasonably justified.

Regarding the POD analysis and using 0.5 as the POF threshold (as listed in Table 3), the results show that the POD was 0.778 when no buffer zone was employed around the landslide points. When the buffer zone radius was increased to 30 m, the POD reached a value of 0.888. Additionally, the ACC increased from 0.672 (no buffer) to 0.835 (30-m buffer). Therefore, the model performance significantly improves with the increase of the buffer zone, as further demonstrated by a detailed presentation of the confusion matrix when a POF of 0.5 is adopted as a threshold.

#### Comparison based on $\%LR_{class}$

To further evaluate the performance of PRL-STIM, the composite index  $LR_{class}$  and  $\%LR_{class}$  were adopted in this study. As shown in Fig. 13a and b, the FS values were classified into five classes from extremely unstable ( $FS < 0.75$ ) to extremely stable ( $FS > 1.50$ ). The majority of landslides were accurately predicted through a comparative analysis between PRL-STIM results and observed landslides. However, the unstable areas were overestimated. The highly unstable zone comprises only 12% of the total area, yet it encompasses up to 23% of the landslides, whereas the highly stable zone accounts for 28% of the total area but exhibits only 5% occurrence of landslides. The unstable areas with  $FS < 1$  constitute only 40% of

total areas when  $FS = 1$  is set as the stability threshold; however, they account for 75% of the total number of observed landslides. Moreover, as shown in Fig. 13c, there is a consistent agreement between the unstable area with continuous rainfall and the PRL-STIM, indicating a trend of gradual change followed by a sudden increase. However, the proportion of unstable areas reaches approximately 58% after a 9-h rainfall forecasted by TRIGRS. In contrast, when employing Scoops3D, around 53% of the total area was identified as unstable. It is also worth noting that the maximum proportion of unstable areas using PRL-STIM accounts for 40% of the total area, while TRIGRS and Scoops3D predict higher proportions of unstable areas, reaching 58% and 53%, respectively. This indicates that the calculated results of PRL-STIM are more conservative. The  $\%LR_{class}$  calculated by PRL-STIM is 81% as presented in Table 4, comparing the values of 71% and 80% reported by TRIGRS and Scoops3D, respectively.

#### Comparison based on computational efficiency

Regarding computational efficiency, we also compared the outcomes of TRIGRS and PRL-STIM. For convenience, the Niangniangba region was once again utilised as the test subject with a raster resolution of  $12.5 \text{ m} \times 12.5 \text{ m}$ , resulting in a total of 71,051 cells within the research area. The results demonstrate that completing a calculation using TRIGRS' infinite-depth model takes approximately 8.8 s, while it takes around 153.7 s for the finite-depth slope calculation model to finish its computation. In comparison, PRL-STIM only requires approximately 0.97 s to complete a deterministic analysis. Furthermore, even when employing the recursive FORM method, the completion of all probability evaluations can be achieved within a mere 17.1 s.

In summary, all these results indicate a satisfactory accuracy for PRL-STIM by comparing the landslide susceptibility map with

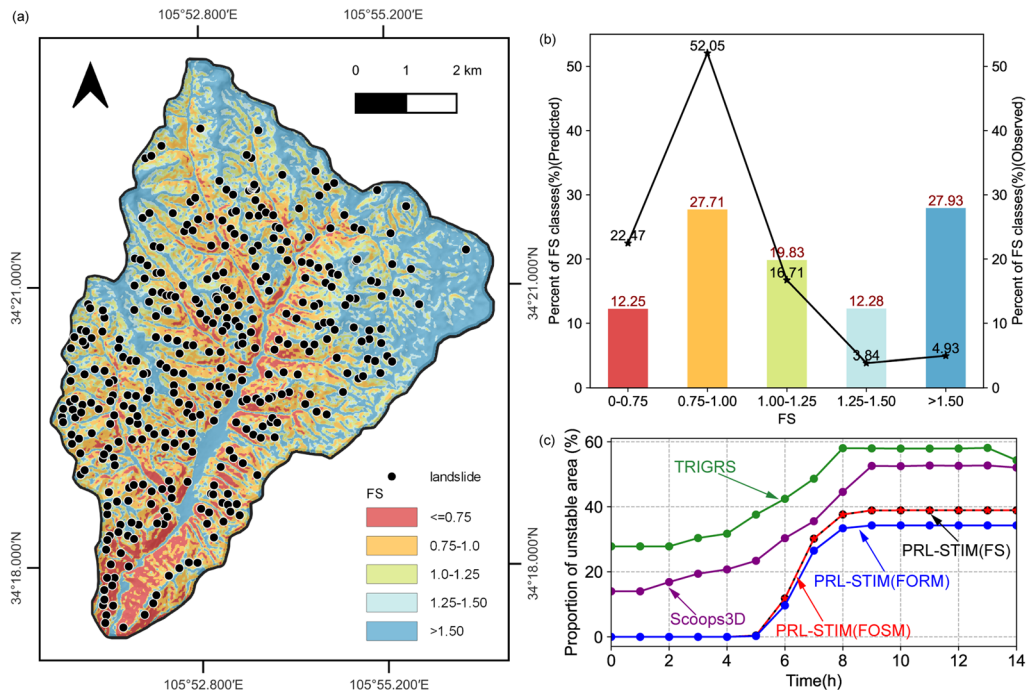


**Fig. 13** Prediction of the spatial distribution of shallow landslides employing PRL-STIM. **a** Map of FS distribution. **b** The proportion of the area of each FS class (observed and predicted). **c** Proportion of predicted unstable area by TRIGRS and Scoops3D

**Table 4** The  $\%LR_{class}$  evaluations utilised to analyse the performance of different models

FS class	% of slides	% of predicted areas	$LR_{class}$	%LR <sub>class</sub>		
				This study	TRIGRS <sup>a</sup>	Scoops3D <sup>a</sup>
FS < 1	74.52	39.96	1.87	81.46	71.28	80.16
FS ≥ 1	25.48	60.04	0.42	18.54	28.72	19.84
Sum	100	100	2.29	100	100	100

<sup>a</sup>Results are provided by He et al. (2021)

observed landslides in the study area. Although different PBM methods cater to diverse requirements and necessitate further case outcomes, the application of our proposed PRL-STIM significantly enhances the landslide susceptibility mapping accuracy and efficiency.

### Challenges and limitations

The challenges and limitations of assessing rainfall-induced shallow landslide susceptibility are undeniable. These primarily include the uncertainty in obtaining accurate physical parameters for regional slope assessments and the limitations related to model assumptions.

The quality of the input data poses a significant limitation to this study, which is a common concern that has been extensively discussed by other researchers in the field of physical-based landslide modelling (Tran et al. 2018; Park et al. 2019; Chen et al. 2020). The primary challenge lies in modelling regional landslide susceptibility assessments, given the uncertainty in acquiring ideal physical parameters that are essential at the regional scale. Nonetheless, some studies, including those using the SPRIn-SL tool based on hydromechanical and geotechnical engineering theories, often treat all input parameters as constants (Raimondi et al. 2023). The outcomes derived from our sensitivity analysis and simulations conducted in the Niangniangba study area underscore the utmost importance of meticulously selecting appropriate parameter values, encompassing saturated permeability, cohesion, friction angle and other pertinent factors. The validation of soil thickness, a critical input parameter for PBM, was not conducted through actual measurements in this study. Instead, predictions were solely based on the soil depth model. The spatial distribution of soil thickness can be highly intricate and is influenced by various geomorphological factors. Consequently, numerous methods have been proposed to predict the spatial distribution of soil depth as discussed in section '**Determination of the soil thickness of shallow landslides**' (Salciarini et al. 2006; Catani et al. 2010; Segoni et al. 2012). While commonly employed for soil thickness determination, it is imperative to acknowledge that basic models such as the S-model and Z-model (Li et al. 2022; Hwang et al. 2023) do not capture the nonlinear nature of soil thickness, as highlighted by Segoni et al. (2012). To address this limitation, Raimondi et al. (2023) utilised polynomial regression and response surface analysis to predict the spatial distribution of soil thickness, while Xiao et al. (2023) proposed the GIST-RF method for effective estimation of soil thickness. Consequently, to enhance the advanced modelling of soil thickness in future versions, it is essential to incorporate a

dedicated module tailored specifically for predicting soil thickness within the current PRL-STIM v1.0 assessment.

Considering the uncertainty of the above-mentioned parameters, the proposed model contains an appropriate approach to address the challenge of obtaining accurate parameter values at regional scales. The FORM-based HLRF-x has proven its advantages by involving less computational cost for the failure probability analysis (Ji et al. 2022). This approach is versatile to landslide probability calculations where the statistics of multiple inputs, the statistical correlation of random variables as well as different probabilistic distributions (such as normal and lognormal distributions) are considered important factors when performing the regional-scale landslide susceptibility mapping. On the other hand, while PRL-STIM's performance validation is based on the TRIGRS model, it is crucial to recognise the inherent diversity in triggering mechanisms between these methodologies. Our PRL-STIM model accounts for the propagation at the wetting front depth, whereas TRIGRS focuses on the rise of the perched water table. This distinction underscores the importance of using models with comparable mechanisms to enhance validation robustness and model efficacy. Nevertheless, the TRIGRS (Baum et al. 2002, 2008) has been extensively used by researchers and acclaimed for its significant contributions to shallow landslide prediction (Bordoni et al. 2015; Viet et al. 2017; Weidner et al. 2018). This also provides a solid foundation for accurate model validation. Our study, situated in Niangniangba, Gansu, China, benefits from abundant data suitable for implementing the TRIGRS model (He et al. 2021; Wang et al. 2022; Zhang et al. 2023; Shao et al. 2023). This creates favourable conditions for conducting comparative validation using the TRIGRS model.

To sum up, the proposed model may facilitate susceptibility mapping in mountainous regions and the implementation of more advanced skills, both conceptual and mathematical. In any case, we would like to emphasize the fact that the PRL-STIM is very useful for practitioners, authorities and decision-makers in landslide susceptibility, hazard and risk zoning in mountainous areas affected by rainfall-induced shallow slope failures. Although numerous tools exist for automated analysis of regional slope stability, these tools typically necessitate multi-platform operation. Our developed PRL-STIM v1.0 is a user-friendly, Windows-based software with broad applicability and portability across diverse geographical regions and environmental conditions.

### Conclusions

Rainfall-induced shallow landslides often result in significant damage and loss of life in mountainous regions. Conducting probabilistic physically-based modelling for regional-scale shallow landslide

susceptibility analysis remains a challenging task. In this study, we propose a simplified transient model for rapid assessment of landslide susceptibility at the regional scale. The model accounts for rainfall infiltration at various time instants and can be effectively integrated with a fast computational framework predicting the probability of landslide failure at the regional scale. This is successfully achieved by implementing a GIS-FORM approach. Moreover, a user-friendly software named ‘PRL-STIM v1.0’ was developed to facilitate convenient utilisation of the model. The key findings can be summarised as follows:

1. The sensitivity analysis quantifies the impact of input parameters on the proposed model. The results indicate that the rainfall intensity ( $I_R$ ), saturated permeability coefficient and soil thickness are the most sensitive physical parameters. Among the remaining parameters of the model, soil cohesion and the internal friction angle exert the greatest influence. This means that small changes in these parameters may significantly affect the predictions of the model. Specifically, the model highlights the significance of rainfall intensity and permeability (notably, the saturated permeability coefficient), which affect water conditions in the soil, within the parameters associated with rainfall conditions. Conversely, when considering the other mechanical properties of soil, particular attention is given to the cohesion and internal friction angle. This suggests that the model considers both rainfall conditions and soil physical properties. Hence, the correctness and variability of these parameters should be carefully evaluated.
2. The prediction accuracy and computational efficiency of the PRL-STIM landslide assessment method were further applied and validated for the July 2013 rainstorm that affected the Niangniangba area and triggered multiple shallow landslides. On the one hand, the calculations confirmed the high computational efficiency of the model, since one run for a total of 711,051 cells and the entire FORM analysis was performed within a mere 17 s. Regarding the comparison between susceptibility maps and the landslide inventory yielded satisfactory outcomes by using the ROC, POD and  $\%LR_{class}$  analysis. When compared to the deterministic-based TRIGRS model as a benchmark, it was observed that the deterministic-based PRL-STIM achieved an AUC value of 0.72. In comparison to an AUC of 0.74 obtained using FOSM, the utilisation of FORM for probabilistic analyses resulted in a superior AUC value of 0.75, along with an estimated  $\%LR_{class}$  of 81.6%. The accuracy of the landslide susceptibility map based on POF reached 89% when a 30-m buffer was applied around the initiation points, while an accuracy of 81% was achieved using FS. This implies that probabilistic analysis is proven to yield slightly more precise results.
3. The application of the PRL-STIM model to predict rainfall-induced shallow landslides in the study area also reveals a strong correlation between unstable areas and the depth of the wetting front. Furthermore, incorporating a 50% probability of failure threshold effectively characterises the spatial distribution of susceptibility to regional landslide hazards. As rainfall continues, there is a gradual increase in the area prone to landslides, which can be accurately predicted using probabilistic analysis models. It should be noted that considering different physical parameters such as COV, statistical correlation and non-normal distribution

significantly impacts the assessment of regional landslide probability.

In conclusion, the proposed PRL-STIM model enables the analysis of spatial distribution and temporal progression of shallow landslides under varying rainfall scenarios. It proves particularly valuable for disaster forecasting, especially in regions with limited data availability. This approach demonstrated satisfying performance and may serve as a fast and straightforward tool for landslide mitigation where data-driven models are not available. However, it is crucial to note that despite the promising initial results exhibited by the PRL-STIM, further investigation is warranted to assess its performance across diverse geographical settings and under varying climatic conditions. Future research should focus on addressing these limitations and exploring the applicability of the PRL-STIM model with more suitable soil-depth prediction models to enhance accuracy and reliability. It is thus hoped that integrating this model into regular works of landslide risk management can contribute significantly to the field of environmental disaster prevention and mitigation.

#### Acknowledgements

Hongzhi Cui acknowledges the financial support of the China Scholarship Council (CSC: 202206710014) for his research at UPC BarcelonaTech. Some software programmes, such as QGIS and Python, are used.

#### Author contribution

Hongzhi Cui: conceptualization, methodology, investigation, writing of original draft which included review and editing. Jian Ji: conceptualization, methodology, writing which included review and editing, and supervision. Marcel Hürlimann: conceptualization, methodology, writing which included review and editing, and supervision. Vicente Medina: conceptualization, methodology review and supervision.

#### Funding

This work is financially supported by the National Natural Science Foundation of China (Grant Nos. U22A20594 and 52079045).

#### Availability of data and material

The datasets used or analysed during the current study are available from the corresponding author on reasonable request.

#### Code availability

Software application.

#### Declarations

**Ethics approval and consent to participate** Not applicable.

**Consent for publication** Not applicable.

**Conflict of interest** The authors declare no competing interests.

## References

- Baum RL, Savage WZ, Godt JW et al (2002) TRIGRS—a Fortran program for transient rainfall infiltration and grid-based regional slope-stability analysis. US Geol Surv Open-File Rep 424:38. <https://doi.org/10.3133/ofr02424>
- Baum RL, Savage WZ, Godt JW (2008) TRIGRS: a Fortran program for transient rainfall infiltration and grid-based regional slope-stability analysis, version 2.0. No.2008-1159. Open-File Report, p 75
- Bordoni M, Meisina C, Valentino R et al (2015) Site-specific to local-scale shallow landslides triggering zones assessment using TRIGRS. Nat Hazard Earth Sys 15:1025–1050. <https://doi.org/10.5194/nhess-15-1025-2015>
- Bordoni M, Vivaldi V, Lucchelli L et al (2021) Development of a data-driven model for spatial and temporal shallow landslide probability of occurrence at catchment scale. Landslides 18:1209–1229. <https://doi.org/10.1007/s10346-020-01592-3>
- Broeckx J, Maertens M, Isabirye M et al (2019) Landslide susceptibility and mobilization rates in the Mount Elgon region, Uganda. Landslides 16:571–584. <https://doi.org/10.1007/s10346-018-1085-y>
- Catani F, Segoni S, Falorni G (2010) An empirical geomorphology-based approach to the spatial prediction of soil thickness at catchment scale. Water Resour Res 46(W05508):5. <https://doi.org/10.1029/2008WR007450>
- Chae B-G, Park H-J, Catani F et al (2017) Landslide prediction, monitoring and early warning: a concise review of state-of-the-art. Geosci J 21:1033–1070. <https://doi.org/10.1007/s12303-017-0034-4>
- Chang Z, Catani F, Huang F et al (2023) Landslide susceptibility prediction using slope unit-based machine learning models considering the heterogeneity of conditioning factors. J Rock Mech Geotech Eng 15:1127–1143. <https://doi.org/10.1016/j.jrmge.2022.07.009>
- Chen Z, Ye F, Fu W et al (2020) The influence of DEM spatial resolution on landslide susceptibility mapping in the Baxie River basin, NW China. Nat Hazards 101:853–877. <https://doi.org/10.1007/s11069-020-03899-9>
- Cui H, Ji J, Song J, Huang W (2022) Limit state line-based seismic stability charts for homogeneous earth slopes. Comput Geotech 146:104749. <https://doi.org/10.1016/j.compgeo.2022.104749>
- Dou J, Yunus AP, Bui DT et al (2020) Improved landslide assessment using support vector machine with bagging, boosting, and stacking ensemble machine learning framework in a mountainous watershed, Japan. Landslides 17:641–658. <https://doi.org/10.1007/s10346-019-01286-5>
- Durmaz M, Hürlimann M, Huvaj N, Medina V (2023) Comparison of different hydrological and stability assumptions for physically-based modeling of shallow landslides. Eng Geol 323:107237. <https://doi.org/10.1016/j.enggeo.2023.107237>
- Emberson R, Kirschbaum D, Stanley T (2021) Global connections between El Nino and landslide impacts. Nat Commun 12:2262. <https://doi.org/10.1038/s41467-021-22398-4>
- Fell R, Corominas J, Bonnard C et al (2008) Guidelines for landslide susceptibility, hazard and risk zoning for land use planning. Eng Geol 102:85–98. <https://doi.org/10.1016/j.enggeo.2008.03.022>
- Gatto MPA, Lentini V, Montrasio L, Castelli F (2023) A simplified semi-quantitative procedure based on the SLIP model for landslide risk assessment: the case study of Gioiosa Marea (Sicily, Italy). Landslides 20:1381–1403. <https://doi.org/10.1007/s10346-023-02040-8>
- Green WH, Ampt GA (1911) Studies on soil physics. J Agric Sci 4:1–24
- Haque U, Blum P, da Silva PF et al (2016) Fatal landslides in Europe. Landslides 13:1545–1554. <https://doi.org/10.1007/s10346-016-0689-3>
- He J, Qiu H, Qu F et al (2021) Prediction of spatiotemporal stability and rainfall threshold of shallow landslides using the TRIGRS and Scoops3D models. CATENA 197:104999. <https://doi.org/10.1016/j.catena.2020.104999>
- Huang W, Leong E-C, Rahardjo H (2018) Upper-bound limit analysis of unsaturated soil slopes under rainfall. J Geotech Geoenvironmental Eng 144:04018066. [https://doi.org/10.1061/\(ASCE\)GT.1943-5606.0001946](https://doi.org/10.1061/(ASCE)GT.1943-5606.0001946)
- Huang W, Loveridge F, Satyanaga A (2022) Translational upper bound limit analysis of shallow landslides accounting for pore pressure effects. Comput Geotech 148:104841. <https://doi.org/10.1016/j.compgeo.2022.104841>
- Huang W, Ding M, Li Z et al (2023) Landslide susceptibility mapping and dynamic response along the Sichuan-Tibet transportation corridor using deep learning algorithms. CATENA 222:106866. <https://doi.org/10.1016/j.catena.2022.106866>
- Hwang I-T, Park H-J, Lee J-H (2023) Probabilistic analysis of rainfall-induced shallow landslide susceptibility using a physically based model and the bootstrap method. Landslides 20:829–844. <https://doi.org/10.1007/s10346-022-02014-2>
- Iverson RM (2000) Landslide triggering by rain infiltration. Water Resour Res 36:1897–1910. <https://doi.org/10.1029/2000WR900090>
- Ji J, Cui H (2023) A GIS-based tool for probabilistic physical modelling and prediction of landslides: improved GIS-TRIGRS-FORM landslide prediction. Geo-Risk 2023. American Society of Civil Engineers, Arlington, Virginia, pp 320–330
- Ji J, Kodikara JK (2015) Efficient reliability method for implicit limit state surface with correlated non-Gaussian variables. Int J Numer Anal Meth Geomech 39:1898–1911. <https://doi.org/10.1002/nag.2380>
- Ji J, Cui H, Zhang T et al (2022) A GIS-based tool for probabilistic physical modelling and prediction of landslides: GIS-FORM landslide susceptibility analysis in seismic areas. Landslides 19:2213–2231. <https://doi.org/10.1007/s10346-022-01885-9>
- Jiang Y, Hu X, Liang H, Ning P, Fan X (2023) A physically based model for the sequential evolution analysis of rainfall-induced shallow landslides in a catchment. Water Resour Res 59:e2022WR032716. <https://doi.org/10.1029/2022WR032716>
- Kaynia AM, Papathoma-Köhle M, Neuhäuser B et al (2008) Probabilistic assessment of vulnerability to landslide: application to the village of Lichtenstein, Baden-Württemberg, Germany. Eng Geol 101:33–48. <https://doi.org/10.1016/j.enggeo.2008.03.008>
- Kendon EJ, Fischer EM, Short CJ (2023) Variability conceals emerging trend in 100yr projections of UK local hourly rainfall extremes. Nat Commun 14:1133. <https://doi.org/10.1038/s41467-023-36499-9>
- Kim J, Lee K, Jeong S, Kim G (2014) GIS-based prediction method of landslide susceptibility using a rainfall infiltration-groundwater flow model. Eng Geol 182:63–78. <https://doi.org/10.1016/j.enggeo.2014.09.001>
- Lee JH, Park HJ (2015) Assessment of shallow landslide susceptibility using the transient infiltration flow model and GIS-based probabilistic approach. Landslides 13:885–903. <https://doi.org/10.1007/s10346-015-0646-6>
- Lee LM, Gofar N, Rahardjo H (2009) A simple model for preliminary evaluation of rainfall-induced slope instability. Eng Geol 108:272–285. <https://doi.org/10.1016/j.enggeo.2009.06.011>
- Li C, Guo C, Yang X et al (2022) A GIS-based probabilistic analysis model for rainfall-induced shallow landslides in mountainous areas. Environmental Earth Sciences 81. <https://doi.org/10.1007/s12665-022-10562-y>
- Liu S, Wang L, Zhang W et al (2023) A physics-informed data-driven model for landslide susceptibility assessment in the Three Gorges Reservoir area. Geosci Front 14:101621. <https://doi.org/10.1016/j.gsf.2023.101621>
- Low B, Tang WH (2007) Efficient spreadsheet algorithm for first-order reliability method. J Eng Mech 133:1378–1387. [https://doi.org/10.1061/\(ASCE\)0733-9399\(2007\)133:12\(1378\)](https://doi.org/10.1061/(ASCE)0733-9399(2007)133:12(1378))
- Lumb P (1962) Effect of rain storms on slope stability. In: Proceedings of the symposium on Hong Kong Soils. Hong Kong: Printed by Local Property & Printing Co., Ltd., pp 73–87
- Marin RJ, Mattos ÁJ (2020) Physically-based landslide susceptibility analysis using Monte Carlo simulation in a tropical mountain basin. Georisk: Assessment and Management of Risk for Engineered Systems and Geohazards 14:192–205. <https://doi.org/10.1080/17499518.2019.1633582>
- Marin RJ, Velásquez MF, Sánchez O (2021) Applicability and performance of deterministic and probabilistic physically based landslide modeling in a data-scarce environment of the Colombian Andes. J South Amer Earth Sci 108:103175. <https://doi.org/10.1016/j.jsames.2021.103175>
- Medina V, Hürlimann M, Guo Z, Antonio L, Jean V (2021) Fast physically-based model for rainfall-induced landslide susceptibility assessment at regional scale. Catena 201:105213. <https://doi.org/10.1016/j.catena.2021.105213>
- Montgomery DR, Dietrich WE (1994) A physically based model for the topographic control on shallow landsliding. Water Resour Res 30:1153–1171. <https://doi.org/10.1029/93WR02979>
- Montrasio L, Valentino R, Losi GL (2011) Towards a real-time susceptibility assessment of rainfall-induced shallow landslides on a regional scale. Nat Hazard Earth Sys 11:1927–1947. <https://doi.org/10.5194/nhess-11-1927-2011>

- Oguz EA, Depina I, Thakur V (2022) Effects of soil heterogeneity on susceptibility of shallow landslides. *Landslides* 19:67–83. <https://doi.org/10.1007/s10346-021-01738-x>
- Pack RT, Tarboton DG, Goodwin CN (1998) The SINMAP approach to terrain stability mapping In: 8th Congress of the International Association of Engineering Geology, Vancouver, British Columbia, Canada
- Park DW, Nikhil NV, Lee SR (2013) Landslide and debris flow susceptibility zonation using TRIGRS for the 2011 Seoul landslide event. *Nat Hazard Earth Sys* 13:2833–2849. <https://doi.org/10.5194/nhess-13-2833-2013>
- Park H-J, Jang J-Y, Lee J-H (2017) Physically based susceptibility assessment of rainfall-induced shallow landslides using a fuzzy point estimate method. *Remote Sensing* 9:487. <https://doi.org/10.3390/rs9050487>
- Park HJ, Jang JY, Lee JH (2019) Assessment of rainfall-induced landslide susceptibility at the regional scale using a physically based model and fuzzy-based Monte Carlo simulation. *Landslides* 16:695–713. <https://doi.org/10.1007/s10346-018-01125-z>
- Pham BT, Pradhan B, Tien Bui D et al (2016) A comparative study of different machine learning methods for landslide susceptibility assessment: a case study of Uttarakhand area (India). *Environ Model Softw* 84:240–250. <https://doi.org/10.1016/j.envsoft.2016.07.005>
- Pradhan B (2013) A comparative study on the predictive ability of the decision tree, support vector machine and neuro-fuzzy models in landslide susceptibility mapping using GIS. *Comput Geosci* 51:350–365. <https://doi.org/10.1016/j.cageo.2012.08.023>
- Rahardjo H, Lim TT, Chang MF, Fredlund DG (1995) Shear-strength characteristics of a residual soil. *Can Geotech J* 32:60–77. <https://doi.org/10.1139/t95-005>
- Rahardjo H, Ong TH, Rezaur RB, Leong EC (2007) Factors controlling instability of homogeneous soil slopes under rainfall. *J Geotech Geoenvironmental Eng* 133:1532–1543. [https://doi.org/10.1061/\(asce\)1090-0241\(2007\)133:12\(1532\)](https://doi.org/10.1061/(asce)1090-0241(2007)133:12(1532))
- Raia S, Alvioli M, Rossi M et al (2014) Improving predictive power of physically based rainfall-induced shallow landslide models: a probabilistic approach. *Geosci Model Dev* 7:495–514. <https://doi.org/10.5194/gmd-7-495-2014>
- Raimondi L, Giacomo P, Marco F, Domenico C, Andrea C (2023) An open-source and QGIS-integrated physically based model for spatial prediction of rainfall-induced shallow landslides (SPRIn-SL). *Environ Model Softw* 160:105587. <https://doi.org/10.1016/j.envsoft.2022.105587>
- Reid ME, Christian SB, Brien DL (2000) Gravitational stability of three-dimensional stratovolcano edifices. *J Geophys Res-Sol Ea* 105:6043–6056. <https://doi.org/10.1029/1999JB900310>
- Reid ME, Christian SB, Brien DL, Henderson ST (2015) Scoops3d- Software to analyze three dimensional slope stability throughout a digital landscape. Technical Report 14-A1. U.S. Geological Survey
- Salciarini D, Godt JW, Savage WZ et al (2006) Modeling regional initiation of rainfall-induced shallow landslides in the eastern Umbria Region of Central Italy. *Landslides* 3:181–194. <https://doi.org/10.1007/s10346-006-0037-0>
- Salciarini D, Fanelli G, Tamagnini C (2017) A probabilistic model for rainfall—induced shallow landslide prediction at the regional scale. *Landslides* 14:1731–1746. <https://doi.org/10.1007/s10346-017-0812-0>
- Saulnier G-M, Beven K, Obled C (1997) Including spatially variable effective soil depths in TOPMODEL. *J Hydrol* 202:158–172. [https://doi.org/10.1016/S0022-1694\(97\)00059-0](https://doi.org/10.1016/S0022-1694(97)00059-0)
- Segoni S, Rossi G, Catani F (2012) Improving basin scale shallow landslide modelling using reliable soil thickness maps. *Nat Hazards* 61:85–101. <https://doi.org/10.1007/s11069-011-9770-3>
- Segoni S, Piculillo L, Gariano SL (2018) A review of the recent literature on rainfall thresholds for landslide occurrence. *Landslides* 15:1483–1501. <https://doi.org/10.1007/s10346-018-0966-4>
- Shao X, Ma S, Xu C, Xu Y (2023) Insight into the characteristics and triggers of loess landslides during the 2013 heavy rainfall event in the Tianshui area. *China Remote Sensing* 15:4304. <https://doi.org/10.3390/rs15174304>
- Silva F, Lambe TW, Marr WA (2008) Probability and risk of slope failure. *J Geotech Geoenvironmental Eng* 134:1691–1699. [https://doi.org/10.1061/\(ASCE\)1090-0241\(2008\)134:12\(1691\)](https://doi.org/10.1061/(ASCE)1090-0241(2008)134:12(1691))
- Simoni S, Zanotti F, Bertoldi G, Rigon R (2008) Modelling the probability of occurrence of shallow landslides and channelized debris flows using GEOTop-FS. *Hydro Process* 22:532–545. <https://doi.org/10.1002/hyp.6886>
- Sun HW, Wong HN, Ho KKS (1998) Analysis of infiltration in unsaturated ground. In: Proceedings of the Annual Seminar on Slope Engineering. Hong Kong: Printed by Local Property & Printing Co., Ltd., pp 101–109
- Tran TV, Alvioli M, Lee G, An HU (2018) Three-dimensional, time-dependent modeling of rainfall-induced landslides over a digital landscape: a case study. *Landslides* 15:1071–1084. <https://doi.org/10.1007/s10346-017-0931-7>
- Viet TT, Lee G, Thu TM, An HU (2017) Effect of digital elevation model resolution on shallow landslide modeling using TRIGRS. *Nat Hazard Rev* 18:04016011. [https://doi.org/10.1061/\(ASCE\)NH.1527-6996.0000233](https://doi.org/10.1061/(ASCE)NH.1527-6996.0000233)
- Wang H, Sun P, Zhang S et al (2022) Evolutionary and dynamic processes of the Zhongzhai landslide reactivated on October 5, 2021, in Niangnianba, Gansu Province, China. *Landslides* 19:2983–2996. <https://doi.org/10.1007/s10346-022-01966-9>
- Weidner L, Oommen T, Escobar-Wolf R et al (2018) Regional-scale back-analysis using TRIGRS: an approach to advance landslide hazard modeling and prediction in sparse data regions. *Landslides* 15:2343–2356. <https://doi.org/10.1007/s10346-018-1044-7>
- Xiao T, Segoni S, Liang X et al (2023) Generating soil thickness maps by means of geomorphological-empirical approach and random forest algorithm in Wanzhou County. *Three Gorges Reservoir Geosci Front* 14:101514. <https://doi.org/10.1016/j.gsf.2022.101514>
- Zhang LL, Zhang J, Zhang LM, Tang WH (2011) Stability analysis of rainfall-induced slope failure: a review. *Proceedings of the Institution of Civil Engineers - Geotechnical Engineering* 164(5):299–316. <https://doi.org/10.1680/geng.2011.164.5.299>
- Zhang J, Huang HW, Zhang LM et al (2014) Probabilistic prediction of rainfall-induced slope failure using a mechanics-based model. *Eng Geol* 168:129–140. <https://doi.org/10.1016/j.enggeo.2013.11.005>
- Zhang S, Zhao L, Delgado-Tellez R, Bao H (2018) A physics-based probabilistic forecasting model for rainfall-induced shallow landslides at regional scale. *Nat Hazard Earth Sys* 18:969–982. <https://doi.org/10.5194/nhess-18-969-2018>
- Zhang X, Ma C, Zhang Y et al (2023) Research on the area-slope relationship of typical rainfall shallow landslides in Xiaolong Mountain forest area of Gansu Province and its influencing factors. *J Soil Water Conserv* 37:54–60. With Chinese abstract.
- Zhang L, Li J, Li X, et al (2016) Rainfall-induced soil slope failure. Stability analysis and probabilistic assessment. Taylor&Francis Group, Florida
- Zizoli D, Meisina C, Valentino R, Montrasio L (2013) Comparison between different approaches to modeling shallow landslide susceptibility: a case history in Oltrepo Pavese, Northern Italy. *Nat Hazard Earth Sys* 13:559–573. <https://doi.org/10.5194/nhess-13-559-2013>

#### Hongzhi Cui Jian Ji (✉)

Geotechnical Research Institute, Hohai University, Nanjing 210024, China

#### Hongzhi Cui

Email: hongzhi\_cui@126.com

#### Jian Ji

Email: ji0003an@e.ntu.edu.sg

#### Hongzhi Cui · Marcel Hürlmann · Vicente Medina

Department of Civil and Environmental Engineering, UPC  
BarcelonaTech, 08034 Barcelona, Spain

#### Hongzhi Cui

Email: hongzhi\_cui@126.com

#### Jian Ji

Key Laboratory of Ministry of Education for Geomechanics and Embankment Engineering, Hohai University, Nanjing, China

#### Jian Ji

Email: ji0003an@e.ntu.edu.sg